PPPL-1930

PPPL--1930

DE82 022231

THE THEORY OF MODE CONVERSION AND WAVE DAMPING NEAR THE ION-CYCLOTRON FREQUENCY

By

P.L. Colestock and R.J. Kashuba

SEPTEMBER 1982

PLASMA PHYSICS LABORATORY

PRINCETON UNIVERSITY
PRINCETON, NEW JERSEY

PREPARED FOR THE U.S. DEPARTMENT OF ENERGY,
UNDER CONTRACT DE-AC02-76-CHO-3073.

NOTICE

Printed in the United States of America.

Available from:

National Technical Information Service
U. S. Department of Commerce
5285 Port Royal Road
Springfield, Virginia 22151

Price: Printed Copy $ * ; Microfische $3.50

*PAGES	NTIS Selling Price
1-25	$5.00
26-50	$6.50
51-75	$8.00
76-100	$9.50
101-125	$11.00
126-150	$12.50
151-175	$14.00
176-200	$15.50
201-225	$17.00
226-250	$18.50
251-275	$20.00
276-300	$21.50
301-325	$23.00
326-350	$24.50
351-375	$26.00
376-400	$27.50
401-425	$29.00
426-450	$30.50
451-475	$32.00
476-500	$33.50
500-525	$35.00
526-550	$36.50
551-575	$38.00
576-600	$39.50

For documents over 600 pages, add $1.50 for each additional 25 page increment.

The Theory of Mode Conversion and Wave Damping Near the Ion-Cyclotron Frequency

P.L. Colestock

Princeton University, Plasma Physics Laboratory

Princeton, New Jersey 08544

R.J. Kashuba

McDonnell-Douglas Astronautics Company

St. Louis, Missouri 63166

Abstract

Using a variational technique, a set of coupled model equations for the mode-conversion process near the ion-cyclotron frequency is derived. The system is truncated to first order in Larmor radius but includes the effects of explicit gradients and a poloidal field. From the equations a conservation rule is extracted which ensures conservation of total energy and provides an explicit expression for the wave damping in differential form. The equations are integrated numerically for the standard cases of fast waves incident from either the low- or high-field sides of the mode-conversion layer. The scaling of the damping processes is discussed and implications for current RF-heating experiments on the Princeton Large Torus are drawn.

In a plasma where two or more propagating waves may coexist, the presence of gradients in the plasma parameters can give rise to localized regions where one mode is strongly coupled or converted to another. This so-called mode conversion process, first pointed out by Stix [1], has received increasing attention in recent years because of its potential importance to the RF heating of thermonuclear plasmas. Mode conversion takes on a special significance when a wave which is accessible from the plasma periphery couples to another wave which can be efficiently damped by the thermal motion of electrons and ions. In particular, recent experimental successes in heating tokamaks near the ion cyclotron frequency have suggested that mode conversion may play a key role in the understanding of the wave damping mechanisms [2-6].

Near the ion cyclotron frequency, mode conversion may take place from the fast magnetosonic wave to an ion Bernstein wave either at the second and higher ion cyclotron harmonics [7,8] or near the two-ion hybrid frequency in a multiple species plasma. Approximate scattering parameters for these cases have been worked out by several authors [9-12], and these results have been recently reviewed by Stix et al. [13]. Early work was based on approximate differential equations derived by neglecting explicit gradient terms and the effects of damping near the mode conversion zone. This work was extended with an elegant treatment by Swanson [14,15], reviewed in Ref. 13, who showed that the presence of strong damping can dominate the mode conversion process. However, as Perkins [9] has pointed out, the effect of a poloidal field in a tokamak (or a gradient in the direction of B) can have a profound influence through a resulting change in the parallel wavelength, and this result has been confirmed in the numerical work of Jacquinot [16]. Moreover, the effects of explicit gradient terms in the wave equations can be expected to modify the results to some degree with regard to wave damping and the conservation of

energy [13]. A totally self-consistent treatment of the mode conversion problem including the above effects and a simple means of calculating wave damping on each particle species have, to date, not appeared.

In this paper our aim is to extend the present theory of mode conversion to provide a quantitative, self-consistent model of the wave damping and its scaling with plasma parameters. An essential element of this analysis is the conservation of total energy and power flow throughout the mode conversion zone. In Section I, we shall derive the wave equations using a variational technique including the effects of gradients along B and strong damping. In Section II, we show that these equations lead to an energy conservation law with explicit expressions for calculating the wave damping for each particle species. In Section III, we outline a straight-forward numerical procedure for solving these equations, and in Section IV we consider the specific case of mode conversion near the ion cyclotron frequency and its harmonics in tokamak plasmas. Finally, a comparison to previous theory is made, and in Section V the implications for ongoing experiments are discussed.

I. Derivation of the Wave Equations

The approach taken in this section is to derive a set of coupled second order equations for the electric fields from a variational principle which is based on a method developed by Berk et al. [17]. In related work, a similar expansion technique was recently applied to this problem by Swanson [18], who reported similar results for the case where ∇B is perpendicular to B. In this work we wish to extend the theory to include more general situations and to provide explicit expressions for the power flow and wave damping.

In the variational method the wave equation is developed in k-space as is done in uniform plasma theory. However, instead of selecting a particular

wave vector, $\underline{k}$, an integration is performed over all $\underline{k}$ values in the direction of the inhomogeneity. The application of the exact variational integral leads to a coupled set of integral equations. A useful approximation scheme exists in which the variational integral is expanded in $\underline{k}$-space and converted to $\underline{x}$-space according to a specific prescription for the ordering of the operators. This approximate integral leads to a coupled set of differential equations which will subsequently be solved numerically.

From Maxwell's equations we can obtain the familiar wave equation

$$\nabla x \left(\nabla \times \underline{E}\right) - k_o^2 \, \underline{E} - \frac{4\pi i\omega}{c^2} \underline{J} = 0 \tag{1}$$

where $\underline{J}$ is determined from the constitutive relation

$$\underline{J} = \underline{\underline{g}} \cdot \underline{E} \quad . \tag{2}$$

For a nonuniform medium, the operator $\underline{\underline{g}}$ is to be understood as an integral operator lacking the property of translational invariance. The ave equation may be derived from the variational integral

$$\int d\underline{x} \, \underline{E}^{+}(\underline{x}) \cdot \left\{ - \nabla x \left[\nabla x \, \underline{E}(\underline{x}) \right] + k_o^2 \, \underline{E}(\underline{x}) + \frac{4\pi i\omega}{c^2} \int d\underline{x}' \, \underline{\underline{g}}(\underline{x},\underline{x}') \, E(\underline{x}') \right\} , \tag{3}$$

where $\underline{E}^{+}$ is the adjoint field satisfying the adjoint of Eq. (3).

If we Fourier decompose the fields, i.e.,

$$\underline{E}(\underline{x}) = \int \frac{d\underline{k}}{(2\pi)^3} \underline{E}(\underline{k})\, e^{i\underline{k} \cdot \underline{x}} \quad , \tag{4}$$

then the variational integral can be recast in $\underline{k}$-space as

$$\int \frac{d\underline{k}}{(2\pi)^3} \left\{ \underline{E}^{+}(-\underline{k}) \cdot \left[\underline{k} \times \left(\underline{k} \times \underline{\underline{I}} \right) + k_o^2 \right] \cdot \underline{E}(\underline{k}) \right.$$

$$\left. + \frac{4\pi i \omega}{c^2} \int \frac{d\underline{k}'}{(2\pi)^3} \underline{E}^{+}(-\underline{k}) \cdot \underline{\underline{\sigma}}(\underline{k}, \underline{k}', \omega) \cdot \underline{E}(\underline{k}') \right\} , \tag{5}$$

where $\underline{\underline{I}}$ is the unit dyadic. In Eq. (4) we take the Fourier decomposition over all three spatial dimensions. It is only necessary to carry the Fourier integral for those directions where the fields are inhomogeneous. Thus for the cases we will be considering, the integral will be done in one and two spatial dimensions. For those directions where there is no spatial variation, a specific wave number, $\underline{k}$, will be chosen.

If the variation of Eq. (5) is taken with respect to $\underline{E}^{+}(-\underline{k})$, then the wave equation in integral form results. However, approximate differential equations can be formulated by expanding the kernel about $\underline{k}$, $\underline{k}' = 0$ which contain the essential physics of mode conversion and which are considerably easier to evaluate numerically. Such an expansion amounts to the usual finite Larmor radius expansion but includes the effects of explicit gradients. For example, in the case of a one-dimensional spatial inhomogeneity considered below, we replace $\underline{\underline{\sigma}}$ by the series

$$\sigma(k, k') = \sum_{n,m}^{N} \sigma^{(n,m)} (k = 0, k' = 0)\, k^n k'^m \quad , \tag{6}$$

where k and k'are in the direction of the inhomogenity. Then the integral in Eq. (5) can be transformed to $\underline{x}$-space by using the transformation

$$\int \frac{dk}{2\pi} k^m E(k) e^{ikx} = (-i)^m \frac{d^m E}{dx^m} \quad . \tag{7}$$

The application of this technique leads to a set of coupled differential equations of the form

$$\frac{d}{dx} \underline{\underline{G}} \frac{d}{dx} \cdot \underline{E} + \underline{\underline{F}} \cdot \frac{d}{dx} \underline{E} + \underline{\underline{H}} \cdot \underline{E} = 0 \quad , \tag{8}$$

where $\underline{\underline{G}}$, $\underline{\underline{F}}$, and $\underline{\underline{H}}$ are matrices whose elements are functions of x. To facilitate the analysis we resolve the $\underline{E}$-vector in components aligned along the local $\underline{B}$-field (ρ,η,ξ) and define another coordinate system (x,y,z) aligned along the gradient as shown in Fig. 1. For definiteness we assume a plasma density and magnetic field variation of the form

$$B_z(x) = B_o\left(1 + \frac{x}{R}\right)^{-1} ,$$

$$B_x(x) = \text{const} , \tag{9}$$

$$n(x) = n_o\left(1 - \frac{x^2 + y^2}{a^2}\right) ,$$

which is appropriate for a narrow zone either side of the mode conversion layer in a tokamak. Oblique incidence and $B_y \neq 0$ effects may be included by taking $k_y \neq 0$, although situations where the gradients are strongly two-dimensional, such as near the plasma periphery, are excluded. We assume n_y and n_z are specified by boundary conditions and are preserved according to

Snell's law consistent with the assumption of a one-dimensional gradient. We note that the procedure outlined here leads to a set of partial differential equations when two-dimensional gradients are considered. The solution of this problem is considerably more involved numerically and will be left to a later work.

The details of the above calculation for specific cases of interest are carried out in the appendix, and we summarize those results here. Including the effects of both fundamental and second harmonic heating, the matrices $\underline{\underline{G}}$, $\underline{\underline{F}}$, and $\underline{\underline{H}}$ are given by

$$\underline{\underline{G}} = \begin{bmatrix} \sin^2\theta - \cos^2\theta\, \tilde{Z}_2 & -i\cos^2\theta\, \tilde{Z}_2 \\ i\cos^2\theta\, \tilde{Z}_2 & 1-\cos^2\theta\, \tilde{Z}_2 \end{bmatrix} \tag{10a}$$

$$\underline{\underline{F}} = \begin{bmatrix} 2ik_z\sin\theta\cos\theta\,(1-\tilde{Z}_2) & -ik_y\cos\theta + 2i\sin\theta\cos\theta\, k_z\tilde{Z}_2 \\ -ik_y\cos\theta + 2i\sin\theta\cos\theta k_z\tilde{Z}_2 & -2ik_z\sin\theta\,\cos\theta\tilde{Z}_2 \end{bmatrix} \tag{10b}$$

and

$$\underline{\underline{H}} = \begin{bmatrix} k_o^2 + k_z^2\cos^2\theta - k_y^2 + k_o^2K_{xxo} + |U|^2\tilde{Z}_2 - \cos\theta U\tilde{Z}_2' & -k_yk_z\sin\theta + k_o^2K_{xyo} - i|U|^2\tilde{Z}_2 + i\cos\theta\, U\tilde{Z}_2' \\ -k_yk_z\sin\theta + k_o^2K_{xyo} + i|U|^2\tilde{Z}_2 - i\cos\theta\, U\,\tilde{Z}_2' & k_o^2 - k_z^2 + k_o^2K_{yyo} + |U|^2\tilde{Z}_2 - \cos\theta\, U\,\tilde{Z}_2' \end{bmatrix} \tag{10c}$$

where $U = ik_z\sin\theta + k_y$

$$K_{xxo} = K_{yyo} = \frac{\omega_p^2}{2k_z v_t \omega \cos\theta} (Z_1 + Z_{-1})$$

and $$K_{xyo} = i \frac{\omega_p^2}{2k_z v_t \omega \cos\theta} (Z_1 - Z_{-1}) \qquad (10d)$$

$$\tilde{Z}_2 = \frac{\omega_p^2}{c^2} \frac{\omega T}{2m\Omega^2} \frac{Z_2}{k_z v_t \cos\theta} .$$

Z_n is the plasma dispersion function evaluated at the n^{th} harmonic. In the above, the parallel electric field, E_ξ, is neglected so that $\underline{E}$ is of the form (E_ρ, E_η); however, E_ξ corrections can be easily included as a perturbation and the resulting matrices are given in the appendix. We note that considerable simplification results when $\theta \to 0$, that is, when there is no component of the gradient along B. Equation (10) forms the starting point for our consideration of the mode conversion problem. If explicit gradients are neglected in the above, the dispersion relation derived from the determinant of the coefficient matrix corresponds to the usual WKB dispersion relation valid to first order in Larmor radius, which has been investigated by previous workers. A generalization of this concept including gradient effects is given in Section III.

II. Energy Conservation Principle

The importance of gradients in the flow of energy has been suggested by Stix [13] and others [19] for the mode conversion problem. This fact is readily apparent from the above results if Eq. (8) is first written in "self-

adjoint" form. Define the vector $\underline{\mathbf{E}}$ by

$$\underline{\mathbf{E}} = \begin{bmatrix} \underline{E} \\ \underline{\underline{G}} \cdot \underline{E}' \end{bmatrix},$$

where the prime denotes differentiation with respect to x. Equation (8) becomes

$$\underline{\underline{P}}_o \cdot \underline{\mathbf{E}}' + \underline{\underline{P}}_1 \cdot \underline{\mathbf{E}} = 0 , \tag{11}$$

where

$$\underline{\underline{P}}_o = \begin{bmatrix} \underline{\underline{F}} & \underline{\underline{I}} \\ -\underline{\underline{I}} & \underline{\underline{O}} \end{bmatrix}$$

$$\underline{\underline{P}}_1 = \begin{bmatrix} \underline{\underline{H}} & \underline{\underline{O}} \\ \underline{\underline{O}} & \underline{\underline{G}}^{-1} \end{bmatrix} .$$

Note that Eq. (11) is formally self-adjoint, i.e., $\underline{\underline{P}}_o = - \underline{\underline{P}}_o^{*t}$, $P_1 = P_1^{*t}$, when $\underline{\underline{F}}$ is antihermitian, and $\underline{\underline{G}}$ and $\underline{\underline{H}}$ are hermitian. This is in fact the case when K_{xxo}, K_{yyo} and $\mathfrak{Z}_2$ are real while K_{xyo} is pure imaginary, that is when damping is zero.

Now for an operator of the form

$$\mathbf{L}\,\underline{u} = \underline{\underline{P}}_o \cdot \underline{u}' + \underline{\underline{P}}_1 \cdot \underline{u} ,$$

it is easily shown that Lagrange's identity [20] for this system is given by

$$\underline{v}^* \cdot \mathbf{L}\underline{u} - \underline{u} \cdot (\mathbf{L}^+\underline{v})^* = \frac{d}{dx} (\underline{v}^* \cdot \underline{\underline{P}}_o \cdot \underline{u}) \quad , \tag{12}$$

where

$$\mathbf{L}^+ \underline{u} = - \underline{\underline{P}}_o^{*t} \cdot \underline{u}' + \underline{\underline{P}}_1^{*t} \cdot \underline{u}$$

is the adjoint operator, and $\underline{u}$ and $\underline{v}$ are any functions in $C^{(1)}$ on the domain. In particular, if we choose $\underline{u} = \underline{v} = \underline{E}$ and use Eq. (11) and its conjugate in Eq. (12), we find the following conservation relation:

$$\frac{d}{dx} (S_x + T_x) = -\{E_L^{*'} U \cos\theta \, (\tilde{Z}_2 - \tilde{Z}_2^*) \, E_L$$

$$+ E_L^{*'} \cos^2\theta \, \tilde{Z}_2 \, E_L' + E_L^* |U|^2 \, \tilde{Z}_2 \, E_L$$

$$+ k_o^2 \, \underline{E}^* \cdot \underline{\underline{K}}_o \cdot \underline{E} - c.c.\} \quad , \tag{13a}$$

where

$$T_x = - E_L^* \cos^2\theta \, \tilde{Z}_2 \, E_L' - E_L^* \cos\theta \, U \, \tilde{Z}_2 \, E_L - c.c. \tag{13b}$$

$$S_x = E_\rho^* \, E_\rho' \sin^2\theta + E_\eta^* \, E_\eta' + E_\rho^* \, (ik_y \cos\theta \, E_\eta + ik_z \sin\theta \cos\theta \, E_\rho) - c.c. \tag{13c}$$

and

$$E_L = E_\rho + iE_\eta \quad .$$

We assert that Eqs. (13b) and (13c) are generalizations of the kinetic and Poynting fluxes respectively to the case of strong gradients and damping. Note that the kinetic flux, Eq. (13b), reduces to the WKB form given by Stix [21] in the limit of sufficiently weak gradients and vanishing absorption. The expression for the Poynting flux, Eq. (13c), is readily shown to be the x-component of $\underline{E} \times \underline{H}^*$, as represented in the (ρ, η, ξ) coordinates. The right hand side of Eq. (13a) represents the losses including both fundamental and cyclotron harmonic damping and is manifestly zero when wave absorption is absent. Thus Eq. (13) represents conservation of energy for the system, and, when the right-hand side is zero, the system is self-adjoint. Once the wave fields have been determined, the wave absorption is easily calculated for each species using Eq. (13a).

III. Numerical Solution Procedure

The wave Eq. (10) can be integrated directly to match given boundary conditions. We adopt two model cases corresponding to a wave of unit amplitude approaching the mode conversion zone on the cold plasma (fast wave) branch from the right or left (Table I). In order to specify the appropriate connection to outer WKB solutions, we consider Eq. (11) and its adjoint

$$\underline{E}' + \underline{\underline{P}}_o^{-1} \cdot \underline{\underline{P}}_1 \cdot \underline{E} = 0 \qquad (14a)$$

$$\underline{E}^{+\prime} - \underline{\underline{P}}_o^{-1*t} \cdot \underline{\underline{P}}_1^{*t} \cdot \underline{E}^+ = 0 \quad . \qquad (14b)$$

Let $\underline{\underline{S}}$ be the matrix which diagonalizes Eq. (14a), i.e.,

$$\underline{\underline{S}}^{-1} \cdot \underline{\underline{P}}_0^{-1} \cdot \underline{\underline{P}}_1 \cdot \underline{\underline{S}} = \underline{\underline{L}} \ ,$$

where $\underline{\underline{L}}$ is a diagonal matrix of eigenvalues. Then letting

$$\underline{\underline{Q}} = \left(\underline{\underline{S}}^{t*} \cdot \underline{\underline{P}}_1^{*t}\right)^{-1} \ ,$$

we find

$$\underline{\underline{Q}}^{-1} \cdot \underline{\underline{P}}_0^{-1*t} \cdot \underline{\underline{P}}_1^{*t} \cdot \underline{\underline{Q}} = \underline{\underline{L}}^{*} \ .$$

Thus $\underline{\underline{Q}}$ diagonalizes the adjoint Eq. (14b), and these eigenvalues are related to those of Eq. (14a) by

$$\lambda^{+} = -\lambda^{*} \ .$$

If we define the vectors $\underline{F}$ and $\underline{G}$ by

$$\underline{\underline{S}} \cdot \underline{F} = \underline{E}$$

$$\underline{\underline{Q}} \cdot \underline{G} = \underline{E}^{+} \ ,$$

we have

$$\begin{aligned} \underline{F}' - \underline{\underline{L}} \cdot \underline{F} &= -\underline{\underline{S}}^{-1} \cdot \underline{\underline{S}}' \cdot \underline{F} \\ \underline{G} + \underline{\underline{L}}^{*} \cdot \underline{G} &= -\underline{\underline{Q}}^{-1} \cdot \underline{\underline{Q}}' \cdot \underline{G} \quad . \end{aligned} \tag{15}$$

When gradients are zero the right-hand side of Eq. (15) is zero, and the solutions reduce to decoupled plane waves. If the right-hand side is kept to first order, however, the usual WKB solutions for the coupled system result, and these may be used to construct the boundary conditions for the numerical integration. Note that the characteristic equation which occurs in the diagonalization of $\underline{\underline{P}}_0^{-1} \cdot \underline{\underline{P}}_1$, namely

$$\left| \underline{\underline{P}}_0^{-1} \cdot \underline{\underline{P}}_1 - \lambda \underline{\underline{I}} \right| = 0 , \tag{16}$$

is a generalization of the uniform plasma dispersion relation to include the effects of gradients.

Referring to Table I, the WKB solutions corresponding to each mode with ingoing or outgoing power (note that the slow wave branch is typically a backward wave) are matched to the numerical solution of Eq. (10) in the following way. Beginning with orthogonal initial conditions, Eq. (10) is integrated numerically four times over the chosen domain. The resulting solution vectors can be used to form a transfer matrix, $\underline{\underline{D}}$, which maps a vector or, say, the high field side into another on the low field side, i.e.,

$$\underline{E}_{LF} = \underline{\underline{D}} \cdot \underline{E}_{HF} .$$

At the domain boundaries we express $\underline{E}$ in terms of the outer WKB solutions, namely

$$\underline{E} = \sum_{j=1}^{4} c_j \underline{S}_j e^{\lambda_j x} ,$$

where $\underline{E}$ and $\underline{S}$ are vectors of the form $\underline{E} = [E_y, E_y', E_x, E_x']$, and the λ_j are the solutions of Eq. (16). Solving for the unknowns in terms of the knowns for each case gives the following expressions for the scattering parameters low field incidence:

$$\frac{E_{trans}}{E_{in}} = \frac{D_{43} + D_{33}}{D}$$

$$\frac{E_{ref}}{E_{in}} = \frac{D_{12}(D_{43} + D_{33}) - D_{13}(D_{32} + D_{42})}{D} \qquad (17)$$

$$\frac{E_{mc}}{E_{in}} = - \frac{D_{42} + D_{32}}{D}$$

with $D = D_{22}(D_{43} + D_{33}) - D_{32}D_{23} - D_{42}D_{23}$

high field incidence:

$$\frac{E_{trans}}{E_{in}} = D_{11} - D_{21} \frac{D_{12}(D_{43} + D_{33}) - D_{13}(D_{32} + D_{42})}{D}$$

$$\frac{E_{ref}}{E_{in}} = - D_{21} \frac{D_{43} + D_{33}}{D} + D_{31} \frac{D_{23}}{D} + D_{41} \frac{D_{23}}{D} \qquad (18)$$

$$\frac{E_{mc}}{E_{in}} = D_{21} \frac{D_{42} + D_{32}}{D} - D_{31} \frac{D_{22}}{D} - D_{41} \frac{D_{22}}{D} \quad .$$

Once all the coefficients c_j are determined, the entire solution in the mode conversion zone may be reconstructed. In terms of the four linearly independent numerical solutions $\underline{\varepsilon}_j = [E_\eta, E_\eta', E_\rho, E_\rho']$, we have

$$\underline{E} = \sum_{j=1}^{4} a_j \underline{\varepsilon}_j \quad .$$

If we let

$$\underline{\underline{T}} = [\underline{\varepsilon}_1, \varepsilon_2, \varepsilon_3, \varepsilon_4,]$$

and

$$\underline{\underline{S}} = [\underline{S}_1, \underline{S}_2, \underline{S}_3, \underline{S}_4] ,$$

where $$\underline{S}_j = \left[1, \lambda_j, \frac{\lambda_j^2 - T_{22}\lambda_j - T_{21}}{T_{23} + \lambda_j T_{24}}, \lambda_j S_{3j}\right] ,$$

then

$$\underline{\underline{D}} = \underline{\underline{S}}^{-1}\Big|_{LF} \cdot \underline{\underline{T}} \cdot \underline{\underline{S}}\Big|_{HF} \tag{19}$$

and

$$\underline{a} = \underline{\underline{T}}^{-1}\Big|_{HF} \cdot \underline{\underline{S}}\Big|_{HF} \cdot \underline{C}\Big|_{HF} .$$

The solution procedure is as follows:

(i) integrate the wave equation with four linearly independent boundary conditions,

(ii) form $\underline{\underline{S}}$ and $\underline{\underline{T}}$; compute $\underline{\underline{D}}$ and the scattering parmeters, c_j,

(iii) compute $\underline{a}$ and then construct $\underline{E}$ by superposition.

Finally, in this section we need to discuss the numerical accuracy of the process. As was pointed out by Swanson [13], the strong evanescense of the

Bernstein wave on the low-field side causes difficulty for numerical integration schemes. The key is to choose a domain wide enough so that the WKB outer solutions are good approximations and yet not so wide that round-off error becomes appreciable due to the rapid growth of the evanescent solution. In practice the domain boundaries can be chosen with some latitude without significant changes in the solution. Moreover, the numerics can be checked in several ways. First, the WKB coefficients can be computed for each point in the domain. When these coefficients are sufficiently slowly varying, the WKB solutions are good representations. This can be checked by varying the domain width to see if the scattering parameters change significantly. Second, the energy conservation relation Eq. (13) gives a convenient check on the accuracy of the integration. The integrated damping should equal the change in total energy across the domain. Finally, if the input power is normalized to unity, the sum of all the remaining powers should be unity. In practice single precision is sufficient for ensuring accuracy of the calculation.

IV. Numerical Results

In the ion cyclotron range of frequencies, the heating regimes fall into two general classes: (i) minority fundamental heating and (ii) second or higher harmonic heating. In the minority heating case, mode conversion may occur at the two-ion hybrid resonance in a multi-species plasma which, if the minority ion is sufficiently dilute, occurs near the fundamental cyclotron layer for the ion. In experiments on the Princeton Large Torus the minority ion regime with either a small component of H or ^{3}He in a Deuterium plasma has shown considerable effectiveness as a means to heat the plasma ions and electrons [4,22].

The results of the numerical solution of the above mentioned system for parameters typical of the H minority regime on PLT are shown in Figs. 2-4. In Fig. 2 the dispersion roots indicate that the Bernstein wave is coupled, although weakly, to the fast wave on the high field side of the H cyclotron layer. Note that the roots are not degenerate or complex conjugate in the mode conversion zone due to the gradient terms which, as it will be seen, affect the strength of the mode converted wave. In the case shown here when $B_x = 0$, the Bernstein wave fields appear primarily in E_ρ which is directed largely along $\underline{k}$ on the Bernstein wave branch. Only a very small fraction of the incident power is mode converted for low field incidence, but minority ion damping is strong for this case and results in virtually complete absorption in a few passes. From the high field side, however, a significant fraction is converted into the backward Bernstein wave which is subsequently lost to electrons through Landau damping as the parallel electric field increases. Note that even though responsible for a large part of the wave damping, the E_ζ field remains much smaller than the perpendicular fields. Note also that the actual wave damping does not follow the shape of the left-handed electric field as would be expected from plane-wave theory due to the interaction of both the kinetic and Poynting fluxes in the damping processes. The effects of altering the minority concentration is shown in Fig. 5. At even modest concentrations of 10% H the reflection coefficient for a low field incident wave increases significantly with a resulting loss in the single pass minority absorption. Coincident with the above the mode conversion efficiency for a high field incident wave increases with a resulting increase in the electron damping. Transmission coefficients for the two cases are similar, in agreement with Ref. 15. Mode conversion efficiency is also an increasing function of density, as shown in Fig. 6. Of some experimental interest is the

fact that the minority ion absorption from the low field side is predicted to remain strong at high density, as shown. Minority ion damping is also expected to increase with increasing temperature, in contrast to expectations of plane wave theory, as shown in Fig. 7. At sufficiently high temperatures the low and high field incidence cases should approach each other. The effect of plasma current (poloidal field) on these results is shown in Fig. 8. For this case a zone slightly off axis is shown, and positive or negative current values correspond to locations above or below the midplane, respectively. In qualitative agreement with the model proposed by Perkins [9], the poloidal field of one sign tends to enhance mode conversion and reduce electron damping through an effective decrease in the local k_ζ value, while the opposite sign decreases mode conversion and increases electron damping. Also in agreement with Perkins, it is found that the asymptotic character of the equations change at sufficiently low plasma pressure and sufficiently high poloidal field values. This case occurs near the plasma periphery in PLT where the one dimensional theory is invalid and will not be treated here. Note that the transmission coefficients for the two standard cases are no longer equal. As a function of the imposed k_z spectrum the minority heating from the low field side indicates a weak maximum at intermediate values, as shown in Fig. 9. Transmission increases at large k_z while reflections appear to decrease. At very low k_z values, absorption decreases while, from the low field side, the reflection coefficient increases significantly. Mode converted waves are predicted to be weakly damped in this case, giving rise to significant power carried by the Bernstein wave. To the extent that this power remains undamped as the Bernstein wave propagates toward regions of ever decreasing wavelength, higher order corrections may have to be included in the equations to determine the ultimate fate of this wave power. A composite map of mode conversion

efficiency for the high field incidence D/H minority case is shown in Fig. 10. It is observed that mode conversion should occur to some extent over a broad range of parameters possible in the PLT experiments.

In the ^{3}He minority case the results are similar to the hydrogen minority case except that the mode conversion and fast wave cutoff are considerably weaker, owing to the different charge-to-mass ratio of the ^{3}He ion. As a consequence, the results are more symmetric for both directions of incidence, and, for a given ^{3}He concentration, wave transmission is larger as shown in Figs. 11 and 12. We note that the relative transparency of the cutoff zone gives rise to significant mode conversion and subsequent electron heating for low field incidence at sufficiently high ^{3}He concentrations.

In the second harmonic heating regime the Bernstein wave is weakly coupled to the fast wave, but the coupling nonetheless has an important influence on the fast wave absorption, as suggested by Takahashi [23] and Hwang et al. [3]. The results for typical PLT parameters which indicate significant second harmonic absorption are shown in Fig. 13. Note that the reflection coefficient for low field incidence is low as a consequence of the fact that the cutoff associated with the fundamental minority cyclotron resonance is absent. The scaling of second harmonic absorption with increasing density and temperature, shown in Figs. 14 and 15, respectively, indicates a favorable extrapolation of this regime to higher beta plasma.

It is useful to compare these results to previous work to ascertain the accuracy of the numerical results and to point out the importance of the gradient effects included in the formulation. A comparison of the present theory to the gradient-free, localized absorption model developed by Swanson indicates that the present work and Swanson's results give similar values for the fast wave scattering parameters, but both of these differ substantially

from the Budden model [9] which does not include damping. In Fig. (16) we observe that the mode converted power is strongly affected by the inclusion of gradient terms, and consequently the strength of damping on the Bernstein branch is affected. While qualitatively the results of this work are similar to Swanson's gradient-free model, quantitatively the mode converted power differs by the factor required to ensure conservation of total energy. Finally, we remark that both the fast wave scattering and Bernstein wave absorption coefficients can be significantly affected by the presence of a poloidal field.

V. Summary and Conclusions

We have derived a set of coupled model equations for mode conversion near the ion cyclotron frequency including the effects of gradients and a poloidal field. The set of equations leads to an energy conservation rule which includes finite Larmor radius effects in differential form. The equations may be integrated directly, yielding the fast wave scattering parameters and the wave absorption by each particle species.

In the case of minority hydrogen heating, strong minority absorption at sufficiently low H concentration is expected for low field incidence over much of the parameter range appropriate on PLT. Electron heating should be feasible with high field incidence associated with mode conversion. Second harmonic heating of deuterium in this regime is expected to remain insignificant under typical conditions. The presence of a poloidal field tends to remove vertical symmetry in the wave damping, due to the increase or decrease in k_ξ at locations above or below the midplane.

The results are qualitatively similar in the ^{3}He minority regime except that mode conversion should play a less important role. Minority ion

absorption is feasible with either direction of incidence, and at sufficiently high ^{3}He concentrations electron heating should occur via mode conversion. It is interesting to note that such heating may be observable for low field incidence owing to the comparatively larger transmission coefficient for this case.

For second harmonic heating it is expected that, even at the relatively low plasma beta values in PLT, the absorption should be significant. Damping is largely independent of direction of incidence for typical parameters and due to the low reflection coefficient from the low field side, central wave absorption should occur in a few passes. Little electron heating in this regime for PLT conditions is expected.

While the above model is appropriate for the core of the plasma, further work is necessary to extend the validity of the analysis to the plasma periphery where the effects of strong poloidal field and two dimensional gradients must be taken into account.

Acknowledgment

The authors wish to acknowledge helpful discussions with a number of workers in this area, including D.G. Swanson, T.H. Stix, S.C. Chu, J.C. Hosea, and J. Jacquinot. Helpful comments from J.R. Wilson and D. Gambier are also appreciated. One of the authors (PLC) was supported by DOE Contract # DE-AC02-76-CHO-3073, and another (R.J. Kashuba) was supported by McDonnell Douglas IRAD funds.

References

[1] STIX, T.H., Phys. Rev. Lett. 15 (1955) 737.

[2] HOSEA, J.C., et al., Phys. Rev. Lett., 43 (1979) 1802.

[3] HWANG, D.L, et al., Proc. Joint Conf. of 4th Inter. Conf. on Plasma Theory and 4th Inter. Congress on Waves and Instabilities in Plasma, Nagoya, Japan, April 7-11, 1980.

[4] HOSEA, J.C., et al., 8th International Conf. on Plasma Physics and Controlled Nuclear Fusion Research, Brussels, [illegible], (1980).

[5] COLESTOCK, P.L., et al., Proc. 2nd Joint Grenoble-Varenna Inter. Symposium on Heating in Toroidal Plasmas, Como, Italy, (1980).

[6] TFR Group, 9th European Conf. on Controlled Fusion and Plasma Physics, Oxford, England (1979).

[7] WEYNANTS, R.R., Rev. Lett. 33 (1974) 78.

[8] SWANSON, D.G., NGAN, Y.C., Phys. Rev. Lett 35 8 (1975) 517.

[9] PERKINS, F.W., Nucl. Fusion 17 6 (1977) 1197.

[10] NGAN, Y.C., SWANSON, D.G., Phys. Fluids 20 11 (1977) 1920.

[11] JACQUINOT, J., MC VEY, B.D., SCHARER, J.E., Nucl. Fusion 17 2 (1977) 88.

[12] SWANSON, D.G., SCHARER, J.E., MC VEY, B.D., MAU, T.K., Nucl. Fusion 17 2 (1977) 297.

[13] STIX, T.H., SWANSON, D.G., Princeton University, Plasma Physics Laboratory Report PPPL-1903; Handbook of Plasma Physics, Vol. I, Galeev, A., Sudan, R.N., North Holland, Amsterdam (to be published).

[14] SWANSON, D.G., Phys. Fluids 21 6 (1978) 926.

[15] SWANSON, D.G., Nucl. Fusion 20 8 (1980) 949.

[16] JACQUINOT J., Varenna-Grenoble Inter. Sym. on Heating in Toroidal Plasmas, Grenoble, France (1980) Vol. I, 127.

[17] BERK, H.L., DOMINGUEZ, R.R., J. Plasma Physics 18 (1977) 31.

[18] SWANSON, D.G., Phys. Fluids 24 11 (1981) 2035.

[19] KUEHL, H.H., OBRIEN, B.B., STEWART, G.E., Phys. Fluids 13 (1970) 1595.

[20] CODDINGTON, E.A., LEVINSON, N., Theory of Ordinary Differential Equations, McGraw-Hill, New York, (1955).

[21] STIX, T.H., Theory of Plasma Waves, McGraw-Hill, New York, (1962).

[22] HOSEA, J.C., et al., Third Joint Varenna-Grenoble Inter. Symposium on Heating in Toroidal Plasmas, Grenoble, France (1982).

[23] TAKAHASHI, H., J. Physique, 38 (1977) Coll. C6, 171.

Appendix

In the appendix we shall derive the wave equations using a variational technique which is an adaptation of a method developed by Berk, et al.[17] We wish to consider cases where there is a component of ∇B along $\underline{B}$. In order to satisfy the divergence condition $\nabla \cdot \underline{B} = 0$, we must assume at least a two dimensional spatial variation. Later we shall specialize to variation along one direction; however, it is convenient to set up the variational integral in the more general form.

A natural choice of coordinate systems for the problem consists of those directions specified by $\underline{B}$ and ∇B at the origin. If we choose $\hat{\xi}$ aligned along $\underline{B}$ and $\hat{\eta}$ perpendicular to the $\underline{B}$ - ∇B plane, the inhomogeneities will be in the $\hat{\rho} - \hat{\xi}$ plane (see Fig. 1).

For this system the linearized perturbed fields are spatially homogeneous in the $\hat{\eta}$-direction, thus in the frame along $\underline{B}$,

$$\underline{E}(\rho,\xi) \exp\{i(\underline{k} \cdot \underline{x} - \omega t)\}$$

$$= \int \frac{dk_\rho}{2\pi} \int \frac{dk_\xi}{2\pi} \underline{E}(\underline{k}) \exp\{i(\underline{k} \cdot \underline{x} - \omega t)\} \quad . \tag{A1}$$

This field may be used in the linearized Vlasov equation to solve for the perturbed current density

$$\underline{J}(\underline{k}) = \int \frac{dk'_\rho}{2\pi} \underline{\underline{g}}(\underline{k}, \underline{k}') \underline{E}(\underline{k}') \ , \tag{A2}$$

where

$$\underline{\underline{g}}\,(\underline{k},\underline{k}') = \sum_s \left(-\frac{q_s^2}{m_s}\right) \int d\rho\, d\xi\, e^{i\{(k_\rho' - k_\rho)\rho + (k_\xi' - k_\xi)\xi\}}$$

$$\cdot \left\{ \int d^3v\, \underline{V} \cdot \left[\frac{i}{\omega} \frac{\partial f^{(s)}}{\partial v_\xi} \hat{\xi} + D\left(f^{(s)}\right) \int_{-\infty}^{t} I(t,t')\, \underline{V}(t')\, dt' \right\} \tag{A3}$$

and

$$\int_{-\infty}^{t} I(t,t')\, \underline{V}(t')\, dt' = \int_{-\infty}^{t} \exp\left\{i\omega(t-t') - \int_{t'}^{t} \underline{k} \cdot \underline{v}\, d\tau\right\} dt'. \tag{A4}$$

In Eq. (A3) the sum over s represents the sum over species type with an unperturbed distribution $f^{(s)}$. The operator D is given by

$$D\left(f^{(s)}\right) = m_s \frac{\partial f^{(s)}}{\partial H} + \frac{\underline{k} \cdot \underline{V}_\xi \hat{\xi}}{\omega} \frac{\partial f^{(s)}}{\partial v_\xi}, \tag{A5}$$

where H is the total energy and v_ξ is the velocity along the magnetic field.

The integral in Eq. (A4) is done over the unperturbed orbits. In performing this calculation we assume that any single particle responds to a constant local magnetic field. This assumption is tantamount to neglecting terms of the order $r_L \nabla B/B$ where r_L is the Larmor radius. Such an ordering may be relaxed to include these higher order terms at the expense of considerably more complexity; however, their contribution to the solution is found to be negligible. The evaluation of the integral in Eq. (A4) yields

$$\int_{-\infty}^{t} I(t,t')\, V_{\xi}(t')\, dt' = i \sum_{N=-\infty}^{\infty} L_N$$

$$\cdot \exp\left\{i\left[k_{\perp}v_{\perp}/\Omega \sin\left(\psi + \theta - \pi/2\right) - N\left(\theta - \pi/2\right)\right]\right\} \underline{S}_N \,, \qquad \text{(A5)}$$

where

$$\underline{S}_N = \begin{bmatrix} v_{\perp} \dfrac{NJ_N}{r_L} \sin\phi - iv_{\perp} J_N' \cos\phi \\ v_{\perp} \dfrac{NJ_N}{r_L} \cos\phi + iv_{\perp} J_N' \sin\phi \\ v_{\xi} J_N \end{bmatrix} \qquad \text{(A6a)}$$

and

$$L_N = \left(\omega - N\Omega - k_{\xi}v_{\xi}\right)^{-1} \,. \qquad \text{(A6b)}$$

The argument of the Bessel function is $k_{\perp}v_{\perp}/\Omega$ where $\perp$ denotes the perpendicular to $\underline{B}$. The angle Ψ is that of $k_{\perp}$ measured from $\hat{\rho}$ in the clockwise direction. The quantity $\underline{g}$ in Eq. (A3) can be modified by considering the transformation

$$\exp\{ik_\perp' r_L \sin(\phi + \Theta - \pi/2)\}$$

$$= \exp\{i \frac{k_\perp' v_\perp}{\Omega} (\sin\phi \cos[\Theta - \pi/2] + \cos\phi \sin[\Theta - \pi/2])\} \tag{A7a}$$

and let Φ be the angle of $k_\perp'$ measured from the $\hat{\rho}$ axis. Then expression (A7a) becomes

$$\exp\{ik_\perp r_L \sin(\Phi + \Theta - \pi/2)\} \exp\left\{-i \frac{v_\perp (k_\rho' - k_\rho) \cos\Theta}{\Omega}\right\} . \tag{A7b}$$

In addition in Eq. (A3) we use

$$\underline{v} \exp\{ik_\perp r_L \sin(\Phi - \Theta - \pi/2)\}$$

$$= \sum_m \exp\{iM(\Phi + \Theta - \pi/2)\} \underline{S}_m^* . \tag{A8}$$

When Eqs. (A5), (A7), and (A8) are combined in Eq. (A3), the integral over in the velocity integral can be done implicitly to eliminate the double sum. In addition we convert from the ρ-coordinate to the guiding-center coordinate y_g,

$$y_g = \rho - \frac{v_\perp \cos\Theta}{\Omega} . \tag{A9}$$

Thus Eq. (A3) becomes

$$\underline{g}\,(\underline{k},\,\underline{k}') = \sum_s \left(-\frac{q_s^2}{m_s}\right) \int dy_g\, d\xi \exp\{i[(k_\rho' - k_\rho)\, y_g + (k_\xi' - k_\xi)\xi\}$$

$$\cdot \int d^3v\, \underline{v} \cdot \hat{\xi}\, \frac{i}{\omega} \frac{\partial f^{(s)}}{\partial v_\xi} \exp\{i\, \frac{v_\perp (k_\rho' - k_\rho) \cos\,\Theta}{\Omega}$$

$$+ i \int d^3v\, D(f^{(s)}) \sum_n L_N\, \underline{S}_N^*\, \underline{S}_N \quad . \tag{A10}$$

We now consider the first velocity integral in Eq. (A10). Because of the v_ξ derivative the only nonzero component is proportional to $\hat{\xi} \cdot \underline{v}$. We also use the integral respresentation

$$J_o(\alpha) = \int \frac{d\,\Theta}{2\pi} \exp\left\{\frac{iv_\perp (k_\rho' - k_\rho) \cos\,\Theta}{\Omega}\right\} , \tag{A11}$$

where $\alpha = (k_\rho' - k_\rho)\, v_\perp/\Omega$. With these substitutions, Eq. (A10) becomes

$$\underline{g}\,(\underline{k},\,\underline{k}') = \sum_s \left(\frac{-iq_s^2}{ms}\right) \int dy_g\, d\xi \exp\; i[(k_\rho' - k_\rho)y_g + (k_\xi' - k_\xi)\xi]$$

$$\cdot \int d^3v \left\{ -\frac{f^{(s)}}{\omega} J_o(\alpha)\, \hat{\xi}\, \hat{\xi} + D(f^{(s)}) \sum_N L_N\, \underline{S}_N^*\, \underline{S}_N \right\} . \tag{A12}$$

The form of Eq. (A12) is symmetric in the k,k' variables except for the L_N term. However, to the order of approximation we shall retain, only the lowest order expression will be required, which is then symmetric in k and k'. This fact is important to ensure that the final system of equations is self-adjoint in the absence of damping.

Referring to the geometry in Fig. 1, we wish to consider the case of an oblique gradient and oblique propagation, i.e., $\Theta \neq 0$. That is, we shall henceforth consider the case of a one dimensional gradient with a component

along the field and secondly a component of the propagation vector perpendicular to the plane of the field and gradient. For this geometry the gradient is aligned along the $\hat{x}$-direction, therefore the integrals in Eqs. (A2) and (A12) along the $\hat{z}$-direction may be immediately performed. Also we shall assume for the moment that $E_\xi = 0$.

In order to obtain specific equations we first expand $\underline{S}_N$, Eq. (A6a), which appears in Eq. (A12). We shall retain only the zeroth order terms in the Larmor radius r_L except for the second harmonic resonant terms, $N = 2$. Then for the ρ,η components we have non-zero contributions

$$\underline{S}_1 = \underline{S}^*_{-1} = -i \begin{bmatrix} 1 \\ i \end{bmatrix} \frac{v_\perp}{2} , \tag{A13}$$

$$\underline{S}_2 = + \begin{bmatrix} 1 \\ i \end{bmatrix} \frac{u_\perp^2}{4\Omega} \left(k_y + i\, k_z \sin\theta + ik_x \cos\theta\right) .$$

We note that each of the quantities is of the form

$$S_{Ni} = \cos\theta + ik_x U_{Ni} . \tag{A14}$$

This fact permits the variational integral, Eq. (5) in the text, to be transformed to x-space, and the result is of the form

$$\int dx\, \underline{E}^+(x) \left[- \nabla x \left(\nabla x \underline{\underline{I}}\right) + k_o^2 \underline{\underline{I}} \right] \cdot \underline{E}(x)$$

$$+ \sum_s \frac{4\pi q_s^2 \omega}{m_s c^2} \int \cdots \int d^3v \sum_N \left\{ \cos\theta\, E_i^+(x) + U_{Ni}^* \frac{dE_i(x)}{dx} \right\}$$

$$D\left(f^{(s)}\right) L_N \left\{ \cos\theta\, E_j(x) + U_{NJ} \frac{dE_j(x)}{dx} \right\} . \tag{A15}$$

In the expression for L_N in Eq. (A6b), k_ξ should be replaced by $k_z \cos\theta$ (the other terms contribute to higher order). The first part of Eq. (A15) may be rewritten

$$\int dx\, E_i^{+}(x) \left\{ - \partial_i \left(\partial_j E_j[x] \right) + \left(\partial_\ell \partial_\ell + k_o^2 \right) E_i(x) \right\} \quad , \tag{A16}$$

where

$$\{\partial x, \partial y, \partial z\} = \left\{ -ik_y,\ -ik_z \sin\theta + \cos\theta \frac{\partial}{\partial x} \ ,\ ik_z \cos\theta + \sin\theta \frac{\partial}{\partial x} \right\} \quad . \tag{A17}$$

All that remains to obtain the equations from Eq. (A15) is the velocity integrals. For the problems discussed here we shall assume the background plasma distribution is Maxwellian. Then

$$D\left(f^{(s)}\right) = - \frac{m}{T} n \left(\frac{m}{2\pi kT} \right)^{3/2} \exp\left\{ - \frac{v^2}{v_t^2} \right\} \quad , \tag{A18}$$

where $v_t^2 = 2kT/m$. Then the v_ξ integral is given by

$$\int dv_\xi f(v_\xi) \frac{-1}{\omega - N\Omega - k_z v_\xi \cos\theta} = \frac{Z(L_N)}{k_z V_t \cos\theta} \quad , \tag{A19}$$

where $L_N = (\omega - N\Omega)/k_z V_t \cos\theta$ and Z is the plasma dispersion function. The $v_\perp$ integrals are of the form

$$\int dv_\perp^2 \, f(v_\perp) \left\{ \begin{array}{l|l} \dfrac{v_\perp^2}{v_t^2} & N = \pm 1 \\ \dfrac{v_\perp^4}{v_t^4} & N = 2 \end{array} \right\} = \begin{array}{l} 1 \\ 2 \end{array} \quad . \tag{A20}$$

If we substitute Eqs. (A18) - (A20) into Eq. (A15), then the mode conversion equations are readily obtained. The E_η equation is found by taking the variation with respect to E_η^+, namely

$$\left(\frac{d^2}{dx^2} - k_y^2 - k_z^2 + k_o^2\right) E_\eta - ik_y \left(ik_y E_\eta + \left[-ik_z \sin\theta + \cos\theta \frac{d}{dx}\right] E_\rho\right)$$

$$= i \sum_s \frac{\omega_p^2}{c^2} \frac{\omega}{2k_z V_t \cos\theta} \left(Z[L_1]\{E_\rho + iE_\eta\} - Z[L_{-1}]\{E_\rho - iE_\eta\}\right)$$

$$+ i \sum_s \beta_s \frac{\omega}{4} \left[ik_z \sin\theta - k_y - \cos\theta \frac{d}{dx}\right] \frac{Z(L_2)}{k_z V_t \cos\theta}$$

$$\cdot \left[-ik_z \sin\theta - k_y + \cos\theta \frac{d}{dx}\right] \left(E_\rho + iE_\eta\right) \quad . \tag{A21}$$

The variation with respect to E_ρ^+ yields

$$\left(\frac{d^2}{dx^2} - k_y^2 - k_z^2 + k_o^2\right) E_\rho - \left(-ik_z \sin\theta + \cos\theta \frac{d}{dx}\right)$$

$$\cdot \left(ik_y E\eta - ik_z \sin\theta \, E\rho + \cos\theta \frac{dE\rho}{dx}\right)$$

$$= - \sum_s \frac{\omega_p^2}{c^2} \frac{\omega}{2k_z V_t \cos\theta} \left(Z[L_1] \{E_\rho + iE_\eta\} + Z[L_{-1}] \{E_\rho - iE_\eta\}\right)$$

$$- i \sum_s \beta_s \frac{\omega}{4} \left[ik_z \sin\theta - k_y - \cos\theta \frac{d}{dx} \right] \frac{Z(L_2)}{k_z V_t \cos\theta}$$

$$\cdot \left[-ik_z \sin\theta - k_y + \cos\theta \frac{d}{dx} \right] \left(E_\rho + iE_\eta \right) \quad . \tag{A22}$$

The first terms on the right hand side of Eqs. (A21) and (A22) correspond to the fundamental resonance. The terms proportional to

$$\beta_s = \frac{\omega_{ps}^2}{c^2} \frac{V_{ts}^2}{\omega_{cs}^2}$$

correspond to the second harmonic resonance. Equations (A21) and (A22) are in the form of Eq. (8) in the text and are readily decomposed to yield the matrices $\underline{\underline{G}}$, $\underline{\underline{F}}$ and $\underline{\underline{H}}$ in Eq. (10) in the text.

The above system is a set of two coupled second order ordinary differential equations. The effects of a small parallel electric field may be included as a perturbation without increasing the order of the system. Neglecting higher order terms E_ξ can be expressed in terms of the perpendicular fields by

$$k_\rho k_\xi E_\rho + k_\eta k_\xi E_\eta + k_o^2 K_{zzo} E_\xi \cong 0 \quad . \tag{A23}$$

If this equation is solved for E_ξ and the result substituted in the ρ-ξ and η-ξ elements of Eq. (A15) the resulting $\underline{\underline{G}}$, $\underline{\underline{F}}$ and $\underline{\underline{H}}$ matrices are perturbed by the following matrices:

$$\underline{\underline{G}}' = \begin{bmatrix} k_z^2\left([\cos^2\theta - \sin^2\theta]^2 - 2\sin^3\theta\cos\theta\right) & -k_y k_z \sin\theta(2\cos^2\theta - \sin^2\theta) \\ -k_y k_z \sin\theta(2\cos^2\theta - \sin^2\theta) & k_y^2 \sin^2\theta \end{bmatrix} \frac{1}{k_o^2 K_{zzo}} \tag{A24a}$$

$$\underline{\underline{F}}' = \begin{bmatrix} 2ik_z^3\sin^2\theta(\sin^2\theta - \cos^2\theta) & ik_y k_z^2(\sin^3 + \cos\theta\sin^2\theta - \cos^3\theta) \\ ik_y k_z^2(\sin^3\theta + \cos\theta\sin^2\theta - \cos^3\theta) & 2ik_y^2\sin\theta\cos\theta k_z \end{bmatrix} \frac{1}{k_o^2 K_{zzo}} \tag{A24b}$$

$$\underline{\underline{H}}' = \begin{bmatrix} -k_z^4\sin^4\theta & -k_y k_z^3\cos\theta\sin^2\theta \\ -k_y k_z^3\cos\theta\sin^2\theta & -k_y^2 k_z^2\cos^2\theta \end{bmatrix} \frac{1}{k_o^2 K_{zzo}} . \tag{A24c}$$

Due to the fact that K_{zzo} is large these perturbations are small and do not appreciably affect the fast wave scattering coefficients. However, on the weakly damped Bernstein wave branch, the resulting small but finite electric field can give rise to strong absorption on electrons.

Figure Captions

Fig. 1 Geometry for the derivation of the wave equations. The magnetic field is in the $\hat{\xi}$ direction, and the $\hat{\rho}$ direction is chosen to lie in the $\underline{B}$ - ∇B plane.

Fig. 2 Eigenvalues of the coefficient matrix for the minority hydrogen heating case, $n_{eo} = 4 \times 10^{13}$ cm^{-3}, $T_{eo} = T_{po} = T_{do} = 2$ keV, $B_o = 29$ kG, $f = 42$ MHz, $k_z = 10$ m^{-1}, $\eta_H = .95$, $\eta_H = .05$, $I_p = 0$ kA, $R_o = 1.32$ m, $a = 0.40$ m. The density profile is parabolic and the temperature profiles are parabolic squared.

Fig. 3 (a) Poynting flux for a wave incident from the high field side, for the parameters of Fig. 2, $P_{tr} = 0.36$, $P_{mc} = .20$, $P_{abs} = .44$; (b) real part (solid) and imaginary part (dashed) of the E_ρ field for high field incidence; (c) corresponding E_η field; (d) corresponding E_ξ field. The fields are normalized to the same but arbitrary scale factor; (e) corresponding left-hand field, long dashed line represents $|E_+|$; (f) absorbed power per unit volume, $P_e = .167$ (solid), $P_d = .01$ (short dash), $P_h = .26$ (long dash); (g) kinetic flux (dash), and total power flux (solid); (h) plane wave decomposition coefficients, right going fast wave (solid), left going fast wave (dash), right going slow wave (short dash), left going slow wave (long dash).

Fig. 4 (a) Poynting flux for a wave incident from the low field side for the parameter of Fig. 2 $P_{tr} = .37$, $P_{ref} = .11$, $P_{mc} = .02$; (b) E_ρ field,

notation is the same as in Fig. 3; (c) E_η field; (d) E_ξ field; (e) left-hand field; (f) absorbed power, P_e = .03, P_d = .03, P_h = .44; (g) kinetic flux and total power flux; (h) plane wave coefficients.

Fig. 5 Scaling with minority hydrogen concentration for PLT parameters. $T_{eo} = T_{po} = T_{do} = 2$ keV, $n_{eo} = 4 \times 10^{13}$ cm^{-3}, $B_o = 29$ kG, $f = 42$ MHz, $k_z = 10$ m^{-1}, $I_p = 0$ kA; (a) low field incidence (LFI), reflected power (solid), transmitted power (dash); (b) absorption for both standard cases, proton damping, LFI (solid), proton damping, HFI (short dash), electron heating via mode conversion, HFI (long dash); (c) high field incidence, HFI, transmitted power (long dash) mode converted power (short dash). defined as the power still propagating on the Bernstein branch at r = 20 cm. B_o was fixed for this calculation.

Fig. 6 Density scaling for the minority hydrogen case in PLT. $n_H = .1$, other parameters are as in Fig. 5. (a) Low field incidence, notation is the same as in Fig. 5, (b) wave absorption, and (c) high field incidence.

Fig. 7 Temperature scaling for the minority hydrogen case in PLT. $T_{eo} = T_{po} = T_{do} = T_\alpha$, other parameters are the same as in Figs. 5 and 6. (a) Low field incidence, (b) wave absorption, and (c) high field incidence.

Fig. 8 Plasma current scaling for the minority hydrogen in PLT. Parameters are the same as in Figs. 5-7, y = 10 cm, (a) low field incidence, (b) wave absorption, (c) high field incidence.

Fig. 9 Parallel wavenumber scaling for the minority hydrogen case in PLT for several plasma current values, other parameters are the same as in Figs. 5-8; (a) low field incidence, (b) wave absorption, and (c) low field incidence.

Fig. 10 Mode conversion scaling for PLT parameters; (a) percentage mode conversion defined as that power which is still propagating on the Bernstein branch at r = 20 cm for fixed density $n_{eo} = 4 \times 10^{13}$ cm^{-3}; (b) percentage mode conversion for fixed parallel wavenumber k_z = 10 m^{-1}.

Fig. 11 Scaling with minority ^{3}He concentration for PLT parameters f = 25 MHz B_o = 25 kG; (a) low field incidence; (b) wave absorption; and (c) high field incidence. Other parameters are the same as in Figs. 5-10 with ^{3}He as the minority species.

Fig. 12 Parallel wavenumber scaling for the ^{3}He minority case (a) low field incidence, (b) wave absorption, and (c) high field incidence.

Fig. 13 Parallel wavenumber scaling for the hydrogen second harmonic case in pure hydrogen for B_o = 14 kG, f = 42 MHz; other parameters are the same as in previous figures. (a) Low field incidence, (b) wave absorption, and high field incidence.

Fig. 14 Density scaling for the hydrogen second harmonic case in PLT. Parameters are the same as for previous figures. (a) Low field incidence, (b) wave absorption, and (c) high field incidence.

Fig. 15 Temperature scaling for the hydrogen second harmonic case in PLT $T_{eo} = T_{po} = T_{\alpha}$. Other parameters are the same as in previous figures. (a) Low field incidence, (b) wave absorption, and (c) high field incidence.

Fig. 16 Comparison of mode conversion and absorption coefficients with (solid) and without (dashed) explicit gradient terms for the minority case depicted in Figs. 5-10.

TABLE 1

	Low Field Incidence		High Field Incidence	
C_j	Left Boundary	Right Boundary	Left Boundary	Right Boundary
Left going Fast $j = 1$	$\frac{E_{trans}}{E_{in}}$	1	$\frac{E_{ref}}{E_{in}}$	0
Right going Fast $j = 2$	0	$\frac{E_{ref}}{E_{in}}$	1	$\frac{E_{trans}}{E_{in}}$
Right going slow $j = 3$	$\frac{E_{mc}}{E_{in}}$	0	$\frac{E_{mc}}{E_{in}}$	0
Left going slow $j = 4$	0	0	0	0

#82X0576

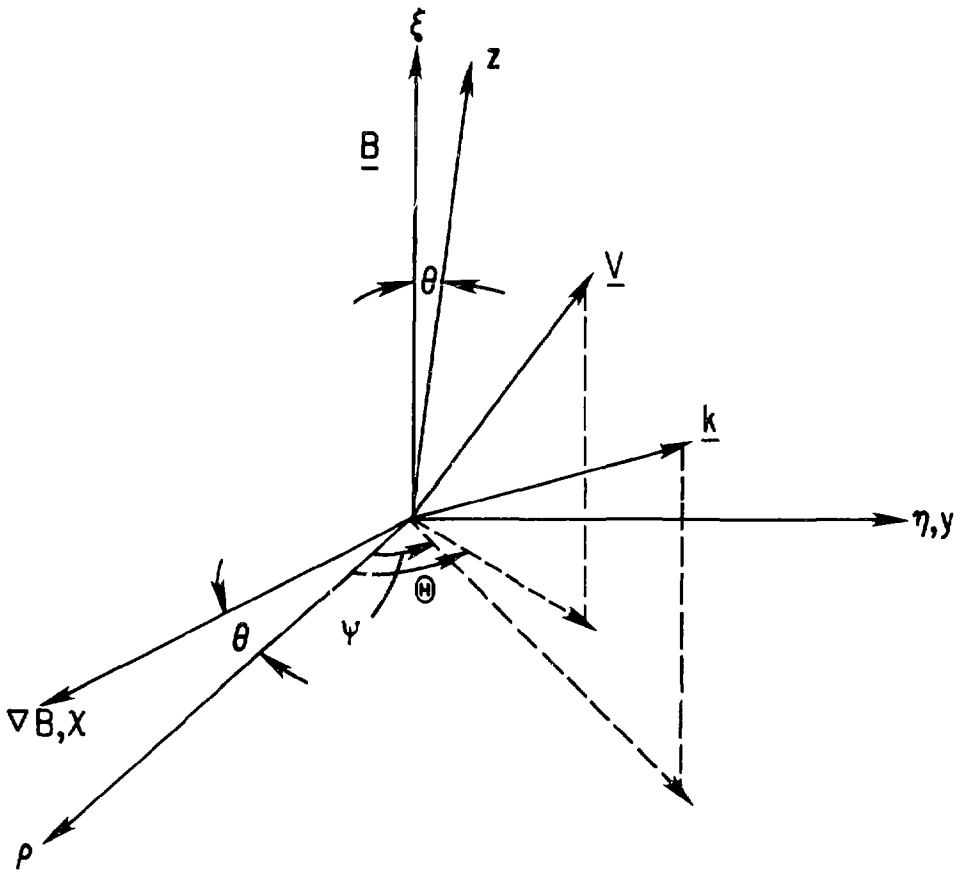

Fig. 1

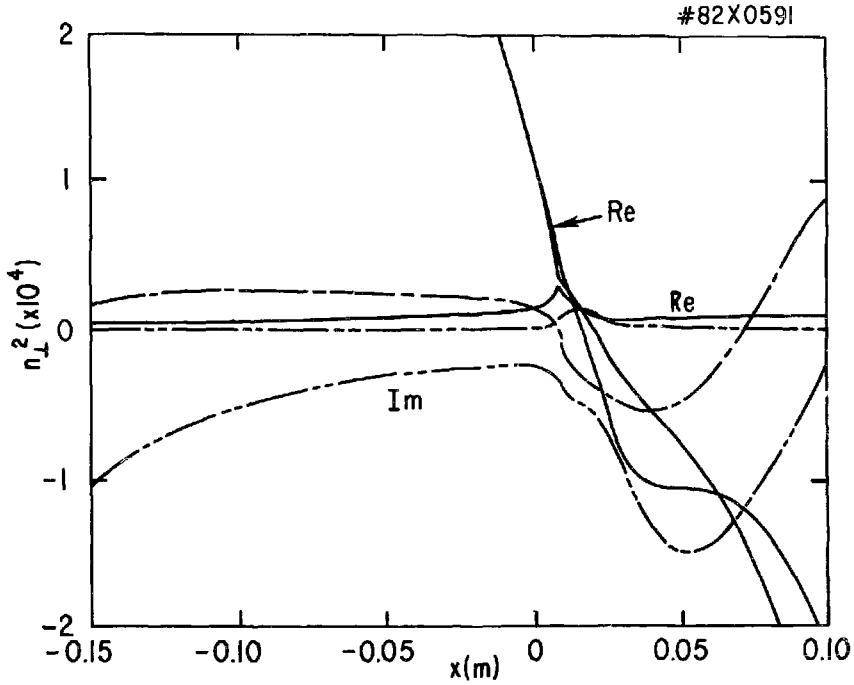

Fig. 2

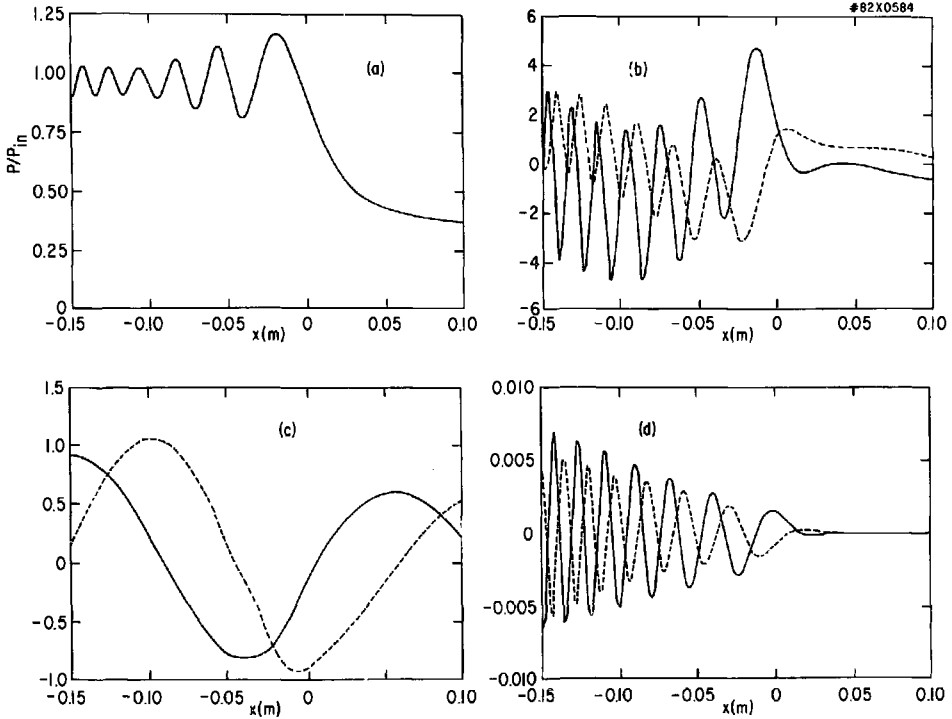
#82X0584
(a)
(b)
(c)
(d)
P/P_in
x(m)
1.25
1.00
0.75
0.50
0.25
0
-0.15
-0.10
-0.05
0.05
0.10
6
4
2
-2
-4
-6
1.5
1.0
0.5
-0.5
-1.0
0.010
0.005
-0.005
-0.010

Fig. 3a

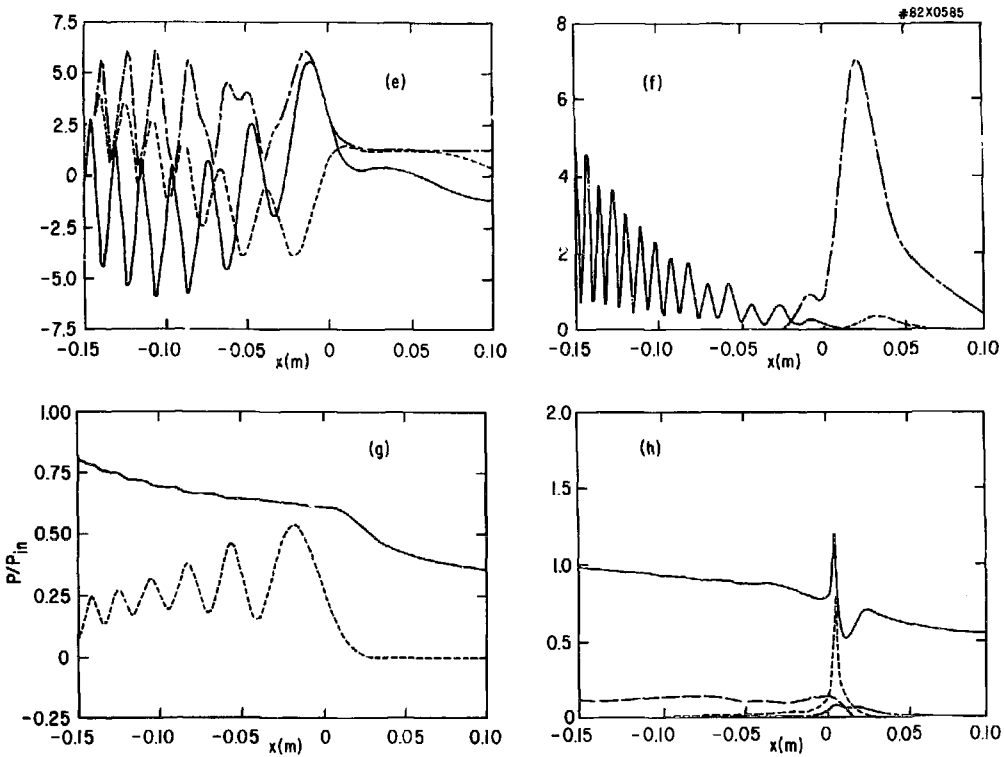

Fig. 3b

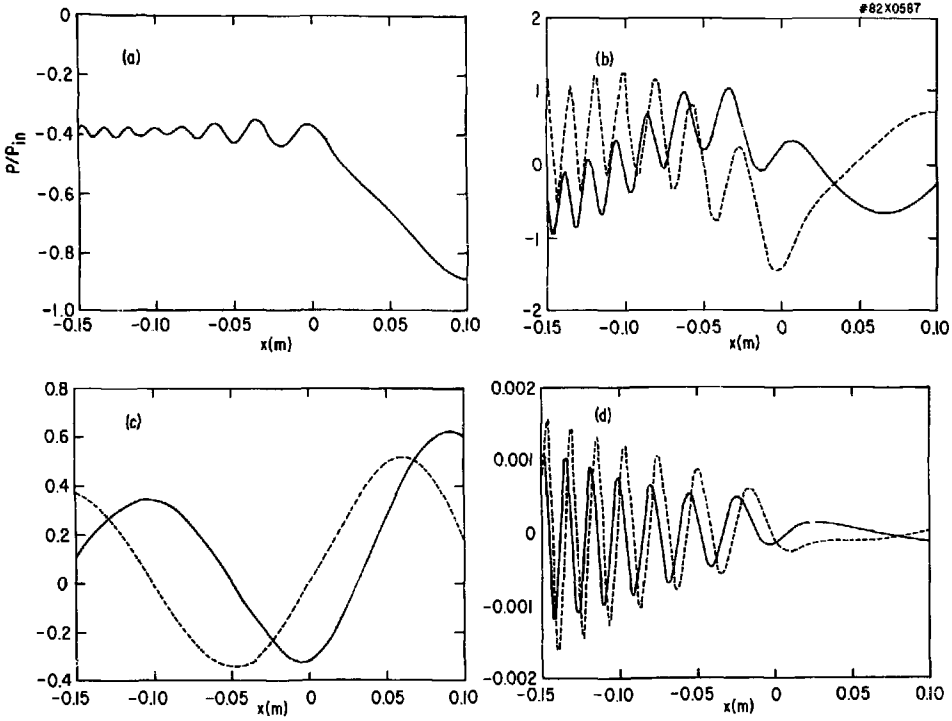
#82X0567
(a)
(b)
(c)
(d)
P/P_in
x(m)
0
-0.2
-0.4
-0.6
-0.8
-1.0
2
1
-1
-2
0.8
0.6
0.4
0.2
-0.4
0.002
0.001
-0.001
-0.002
-0.15
-0.10
-0.05
0.05
0.10

Fig. 4a

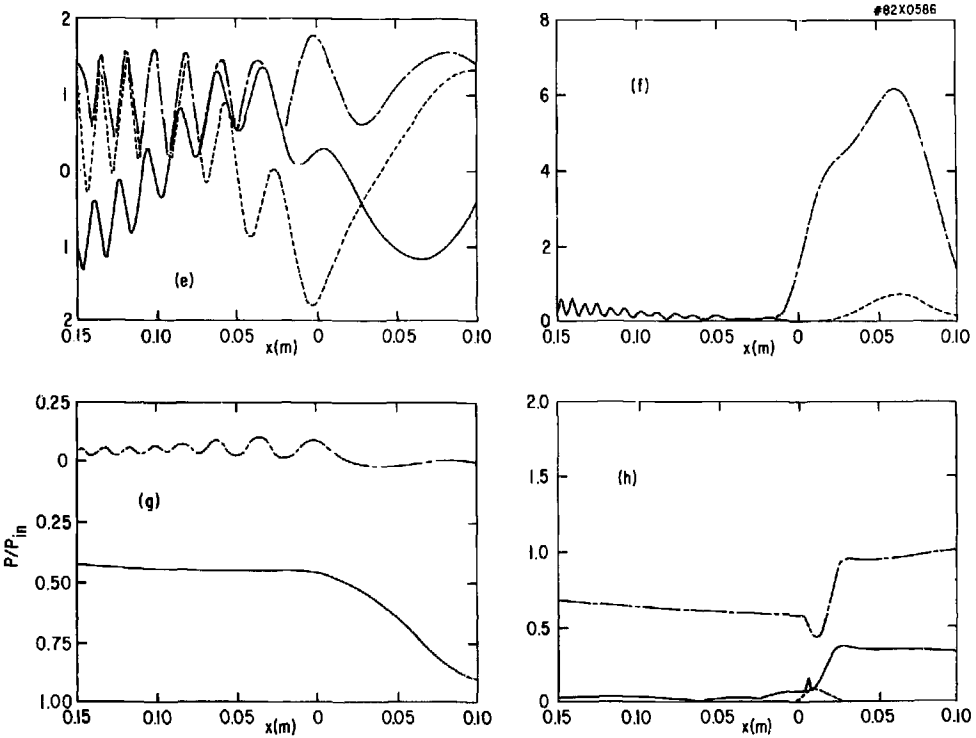

Fig. 4b

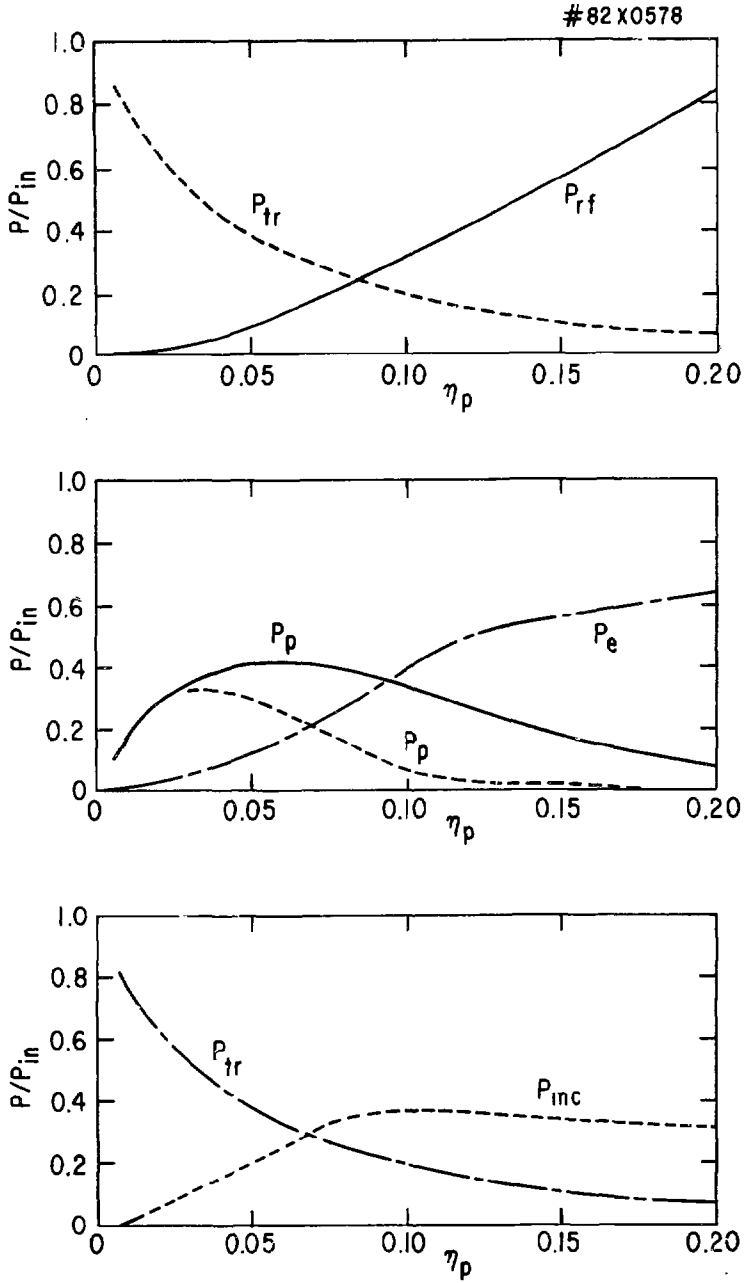
#82X0578
P/Pin
1.0
0.8
0.6
0.4
0.2
0
0
0.05
0.10
0.15
0.20
ηp
Ptr
Prf
Pp
Pe
Pp
Ptr
Pinc

Fig. 5

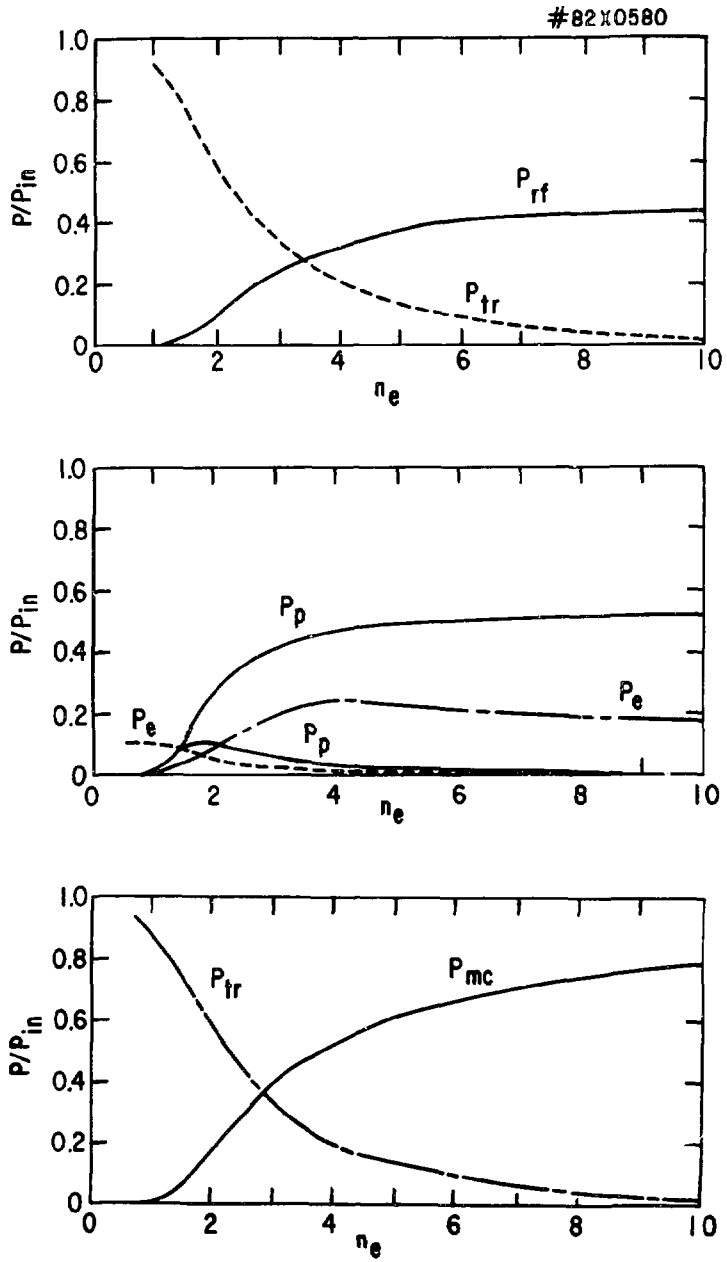

Fig. 6

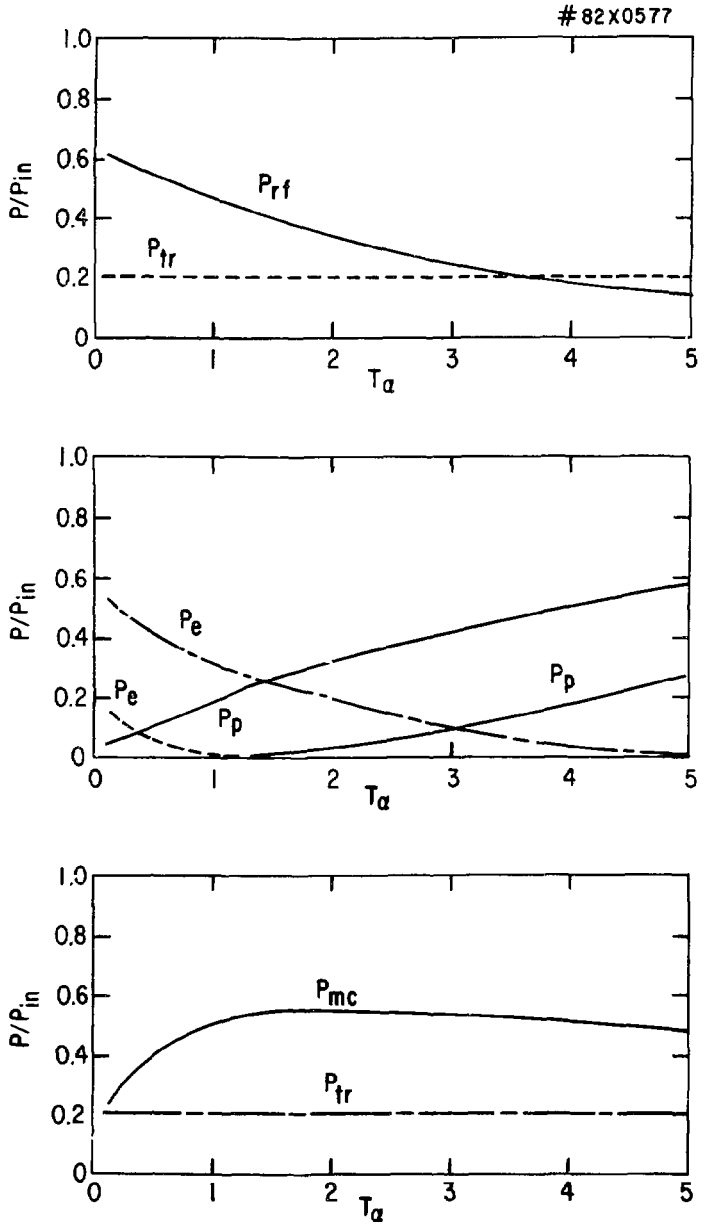

Fig. 7

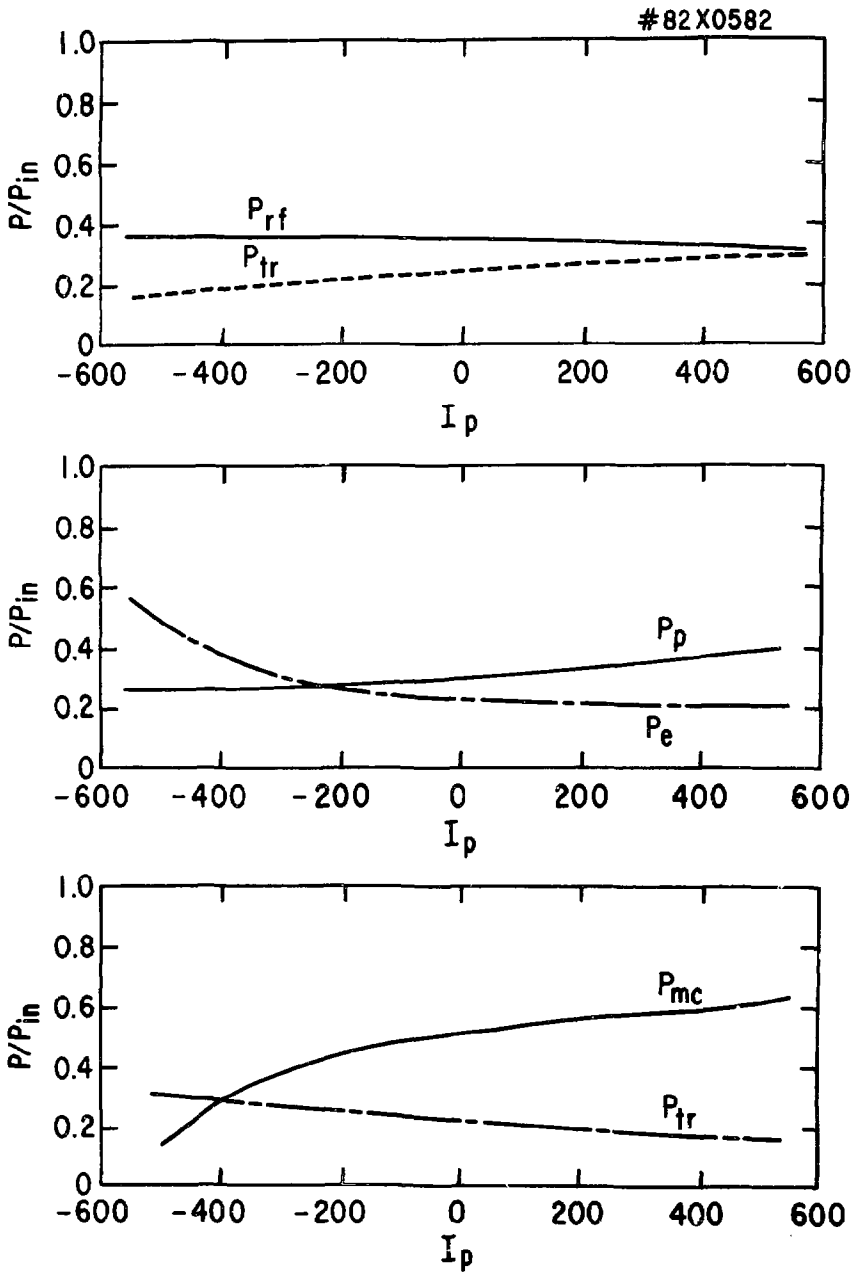
#82X0582
1.0
0.8
0.6
0.4
0.2
0
P/Pin
Prf
Ptr
-600
-400
-200
0
200
400
600
Ip
Pp
Pe
Pmc

Fig. 8

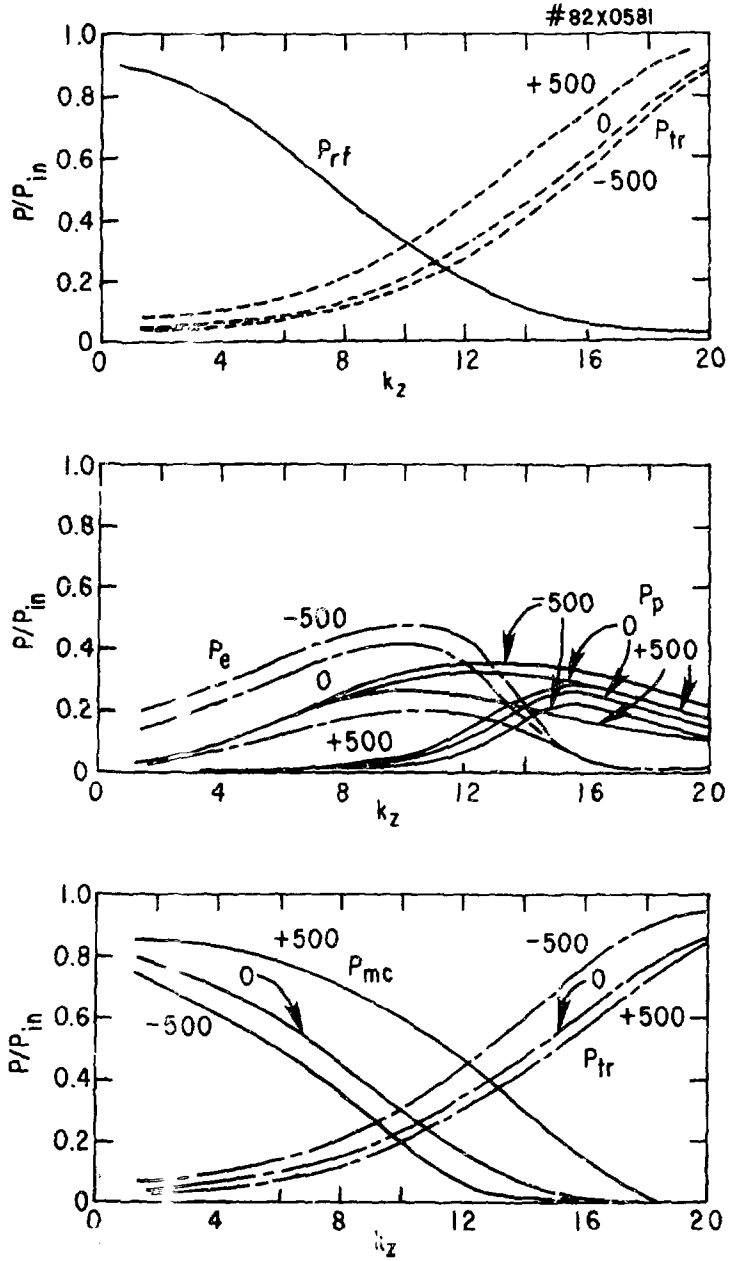

Fig. 9

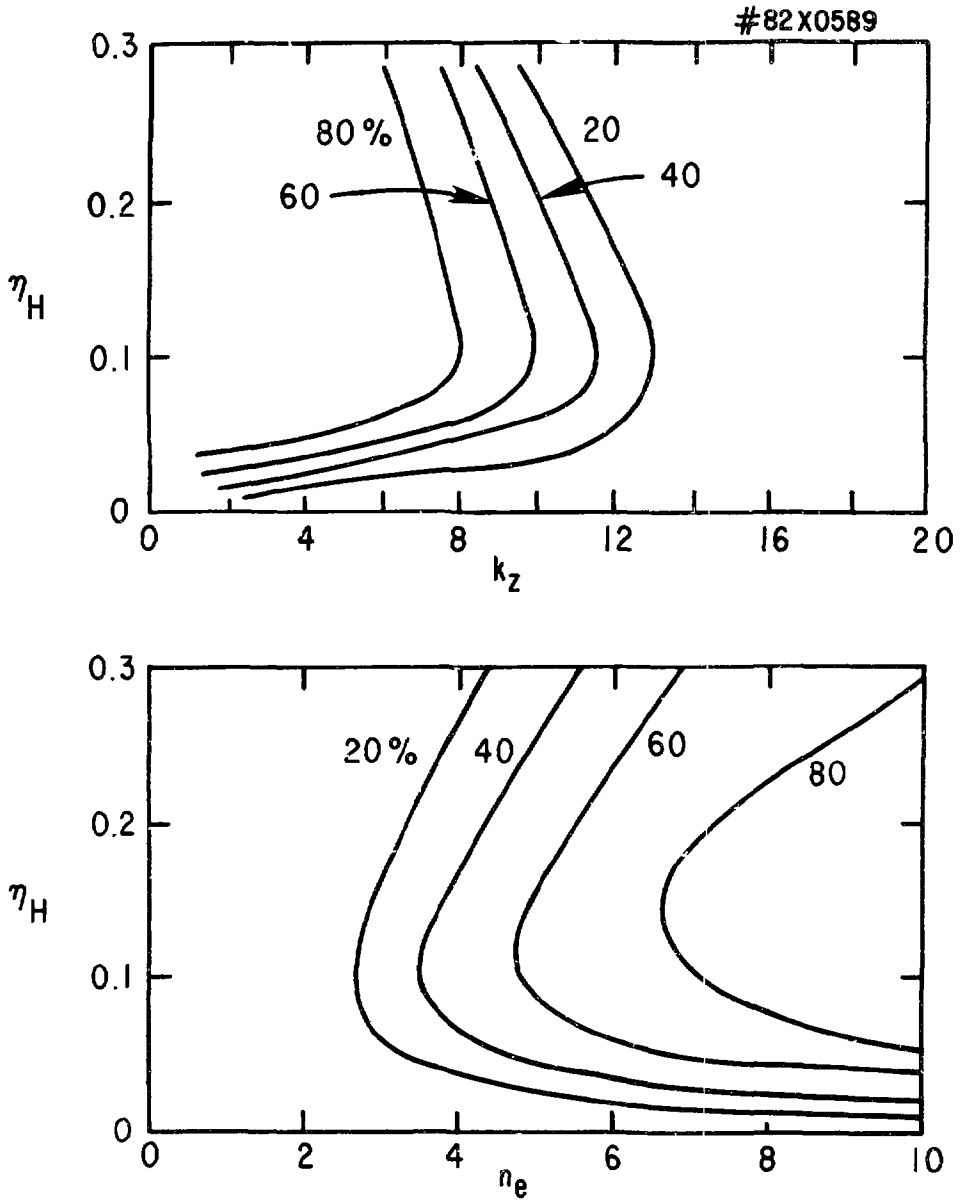
#82X0589
0.3
0.2
0.1
0
η_H
80%
60
20
40
0
4
8
12
16
20
k_z
0.3
0.2
0.1
0
η_H
20%
40
60
80
0
2
4
6
8
10
n_e

Fig. 10

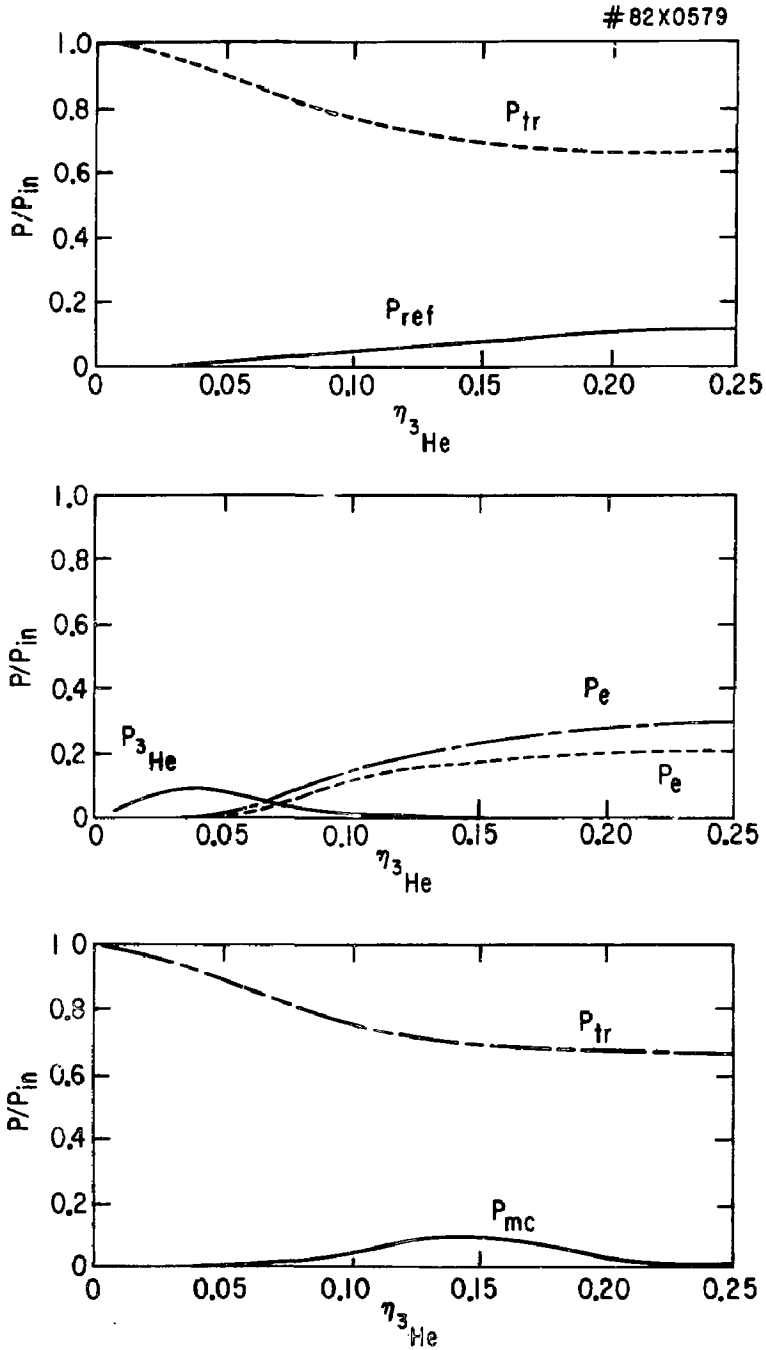
#82X0579
P/Pin
1.0
0.8
0.6
0.4
0.2
0
Ptr
Pref
0
0.05
0.10
0.15
0.20
0.25
η3He
P/Pin
P3He
Pe
Pe
η3He
P/Pin
Ptr
Pmc
η3He

Fig. 11

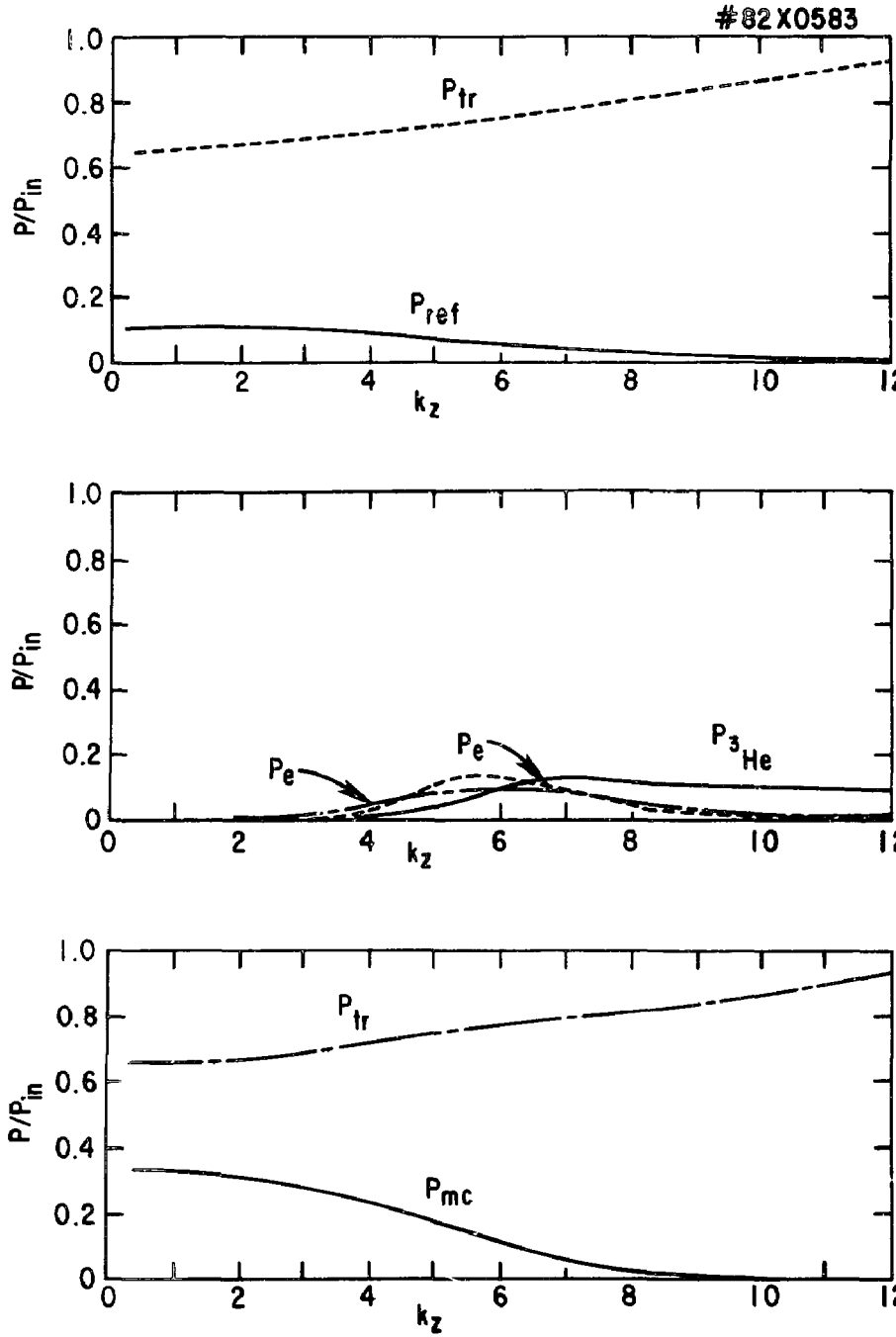
#82X0583
P/Pin
1.0
0.8
0.6
0.4
0.2
0
Ptr
Pref
0
2
4
6
8
10
12
kz
P/Pin
Pe
Pe
P3He
kz
P/Pin
Ptr
Pmc
kz

Fig. 12

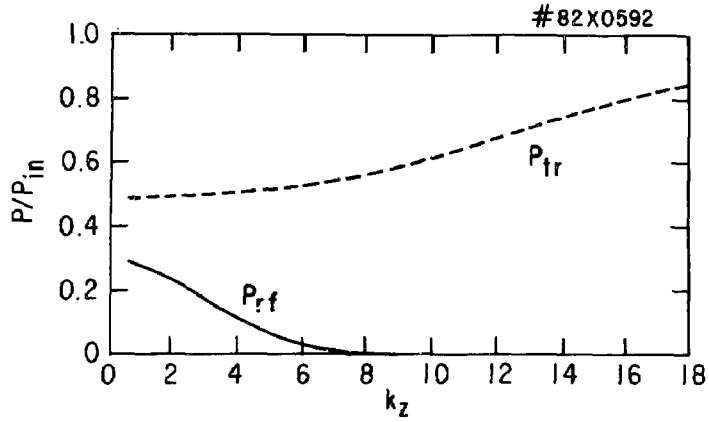
#82X0592
1.0
0.8
0.6
0.4
0.2
0
P/P_in
P_tr
P_rf
0 2 4 6 8 10 12 14 16 18
k_z

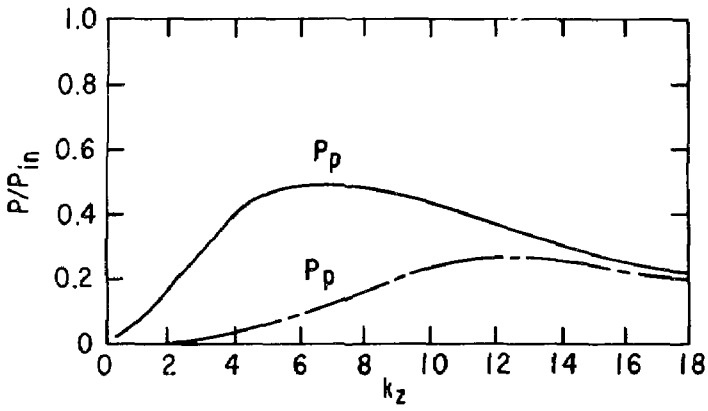
1.0
0.8
0.6
0.4
0.2
0
P/P_in
P_p
P_p
0 2 4 6 8 10 12 14 16 18
k_z

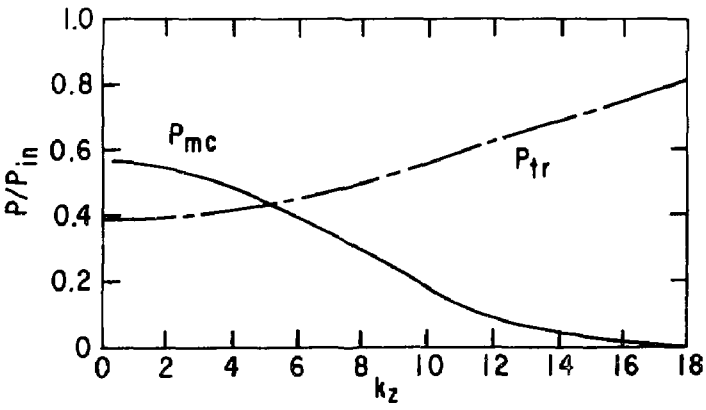
1.0
0.8
0.6
0.4
0.2
0
P/P_in
P_mc
P_tr
0 2 4 6 8 10 12 14 16 18
k_z

Fig. 13

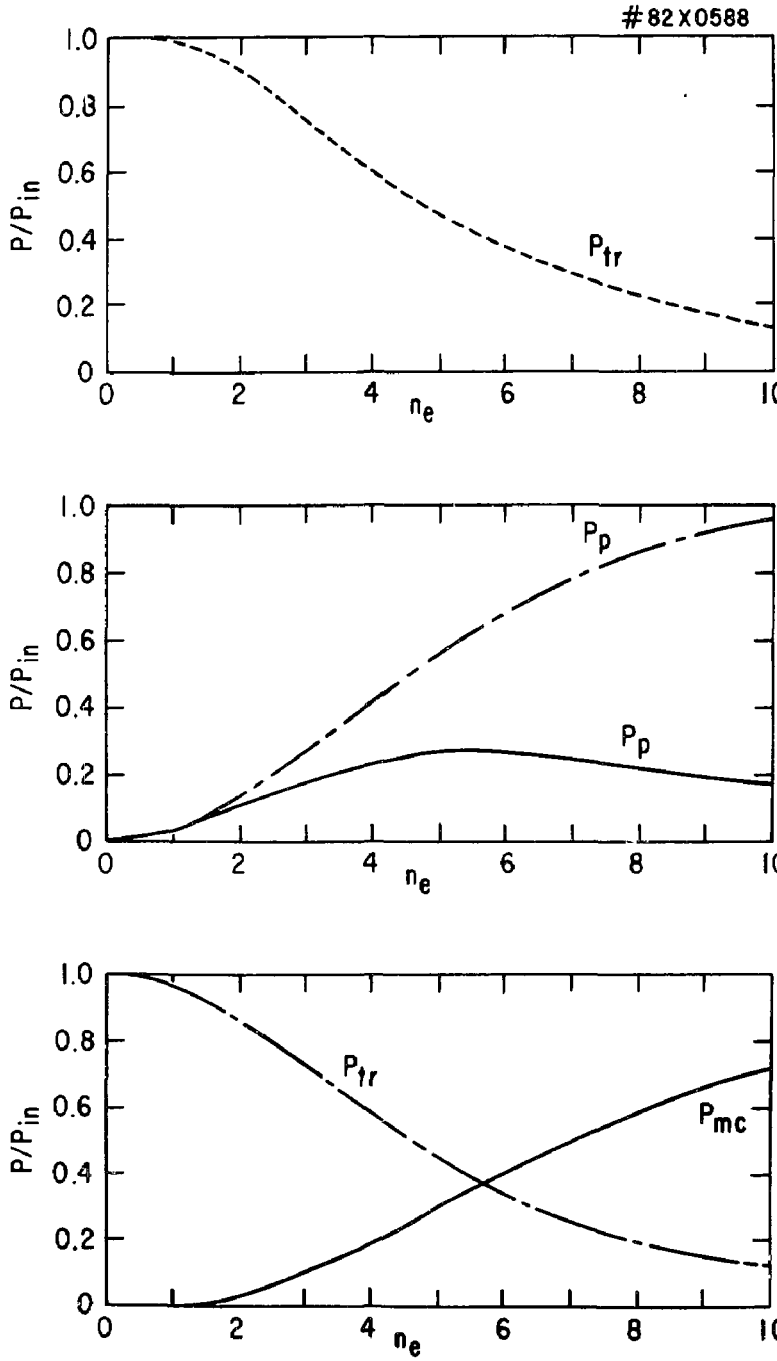

Fig. 14

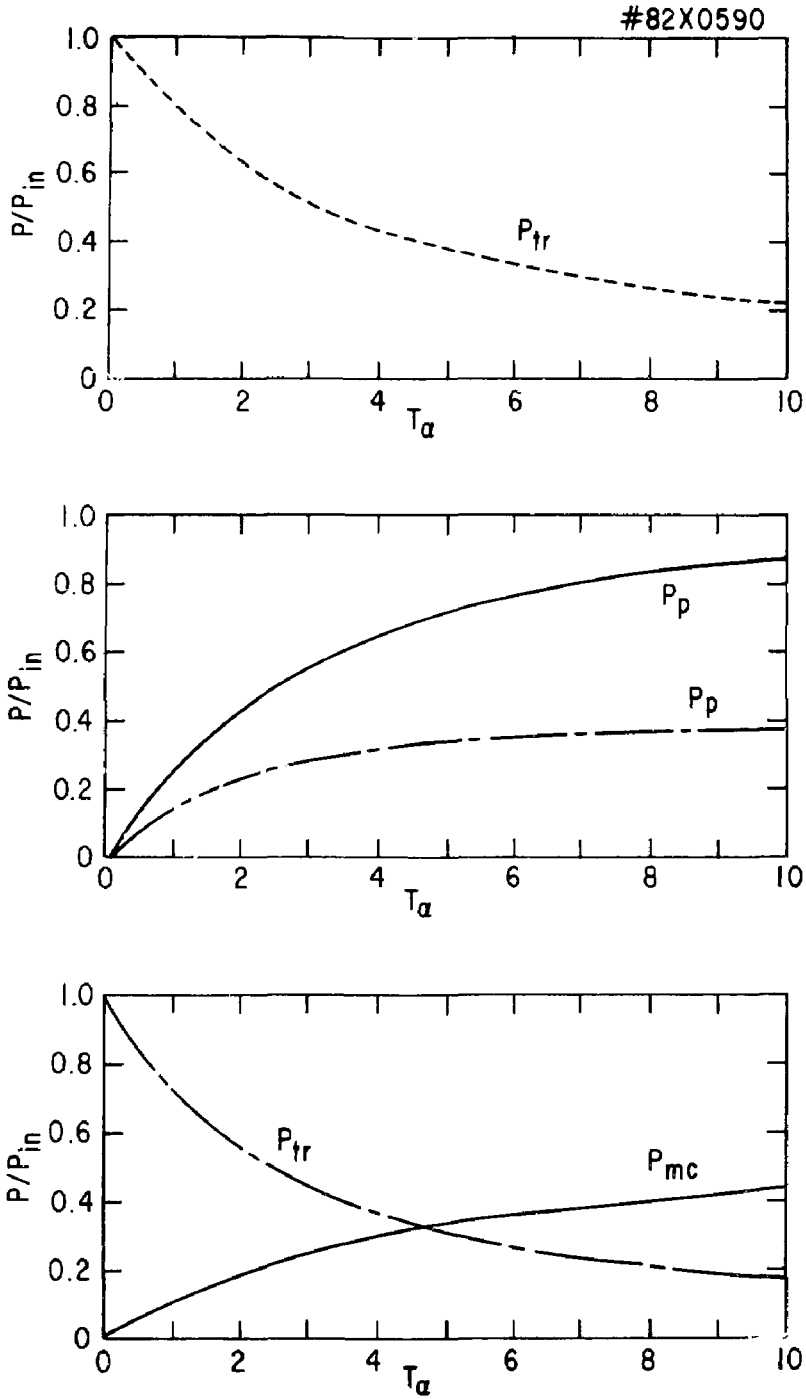

Fig. 15

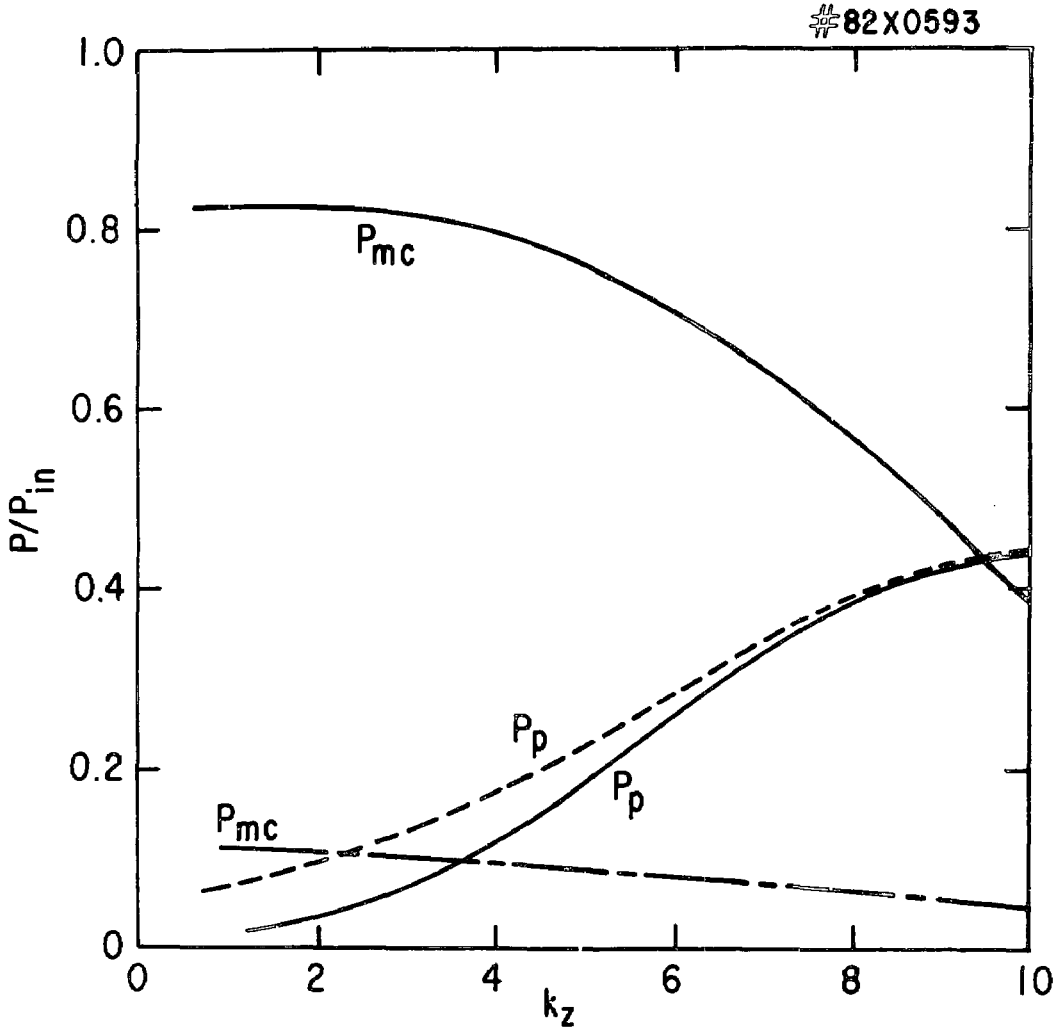

Fig. 16